Changes in Tropical Cyclone Activity due to Global Warming: Results from a High-Resolution Coupled General Circulation Model

S. GUALDI

Istituto Nazionale di Geofisica e Vulcanologia, Bologna, and Centro Euro-Mediterraneo per i Cambiamenti Climatici, Lecce, Italy

E. SCOCCIMARRO

Istituto Nazionale di Geofisica e Vulcanologia, Bologna, Italy

A. NAVARRA

Istituto Nazionale di Geofisica e Vulcanologia, Bologna, and Centro Euro-Mediterraneo per i Cambiamenti Climatici, Lecce, Italy

(Manuscript received 28 February 2007, in final form 7 April 2008)

ABSTRACT

This study investigates the possible changes that greenhouse global warming might generate in the characteristics of tropical cyclones (TCs). The analysis has been performed using scenario climate simulations carried out with a fully coupled high-resolution global general circulation model. The capability of the model to reproduce a reasonably realistic TC climatology has been assessed by comparing the model results from a simulation of the twentieth century with observations. The model appears to be able to simulate tropical cyclone–like vortices with many features similar to the observed TCs. The simulated TC activity exhibits realistic geographical distribution, seasonal modulation, and interannual variability, suggesting that the model is able to reproduce the major basic mechanisms that link TC occurrence with large-scale circulation. The results from the climate scenarios reveal a substantial general reduction of TC frequency when the atmospheric CO_2 concentration is doubled and quadrupled. The reduction appears particularly evident for the tropical western North Pacific (WNP) and North Atlantic (ATL). In the NWP the weaker TC activity seems to be associated with reduced convective instabilities. In the ATL region the weaker TC activity seems to be due to both the increased stability of the atmosphere and a stronger vertical wind shear. Despite the generally reduced TC activity, there is evidence of increased rainfall associated with the simulated cyclones. Finally, the action of the TCs remains well confined to the tropical region and the peak of TC number remains equatorward of 20° latitude in both hemispheres, notwithstanding the overall warming of the tropical upper ocean and the expansion poleward of warm SSTs.

1. Introduction

Tropical cyclones (TCs) are nonfrontal synoptic-scale low pressure systems, which develop over warm pools of the tropical or subtropical oceans and have organized convection and a distinct cyclonic surface wind circulation (Holland 1993). Severe tropical cyclones, also known as "hurricanes" in the North Atlantic and northeast Pacific and "typhoons" in the west Pacific, are one of the most devastating natural phenomena, which often cause severe human and economic losses. Therefore, understanding of the mechanisms that underlie their formation and evolution has been considered a high priority from the scientific, social, and economic points of view.

The increased frequency and intensity of observed hurricanes since 1995 (Goldenberg et al. 2001; Webster et al. 2005) and the extraordinary nature of the North Atlantic hurricane season that occurred in 2005 have triggered considerable debate about the possible changes of TC frequency and intensity resulting from global climate change (e.g., Emanuel 2005; Trenberth

Corresponding author address: Dr. Silvio Gualdi, Aldo Moro 44, 40127 Bologna, Italy.
E-mail: gualdi@bo.ingv.it

DOI: 10.1175/2008JCLI1921.1

2005; Pielke et al. 2005; Anthes et al. 2006; Pielke et al. 2006; Landsea et al. 2006; among others).

A number of studies have shown that TC activity varies substantially from interannual to decadal time scales. For example, the sensitivity of the TC activity to the phase of El Niño–Southern Oscillation (ENSO) has been documented in several studies (e.g., Gray 1984; Chan 2000; Chia and Ropelewski 2002). Similarly, low-frequency modulations of the North Atlantic Oscillation (NAO) exert significant influence on the behavior of TCs (e.g., Elsner and Kocher 2000).

The large interannual and decadal changes associated with natural modes of climate variability make the identification of changes in the TC features that could be unambiguously attributed to the global warming (Walsh 2004) difficult. The detection of possible trends becomes even harder when observational datasets are used. It is the destructive nature of TCs that makes the collection of observed data extremely difficult and expensive. For this reason, databases of observed TCs are available only for a few regions (particularly North Atlantic) and are generally limited in length. Furthermore, because of subjective measurements and variable procedures, the reliability of the existing tropical cyclone databases for estimating climatological trends has been questioned (Landsea et al. 2006; Landsea 2007).

To overcome the limitations of the observational datasets, the possible influence of global warming on TC activity also has been explored using numerical models. Since the early work of Broccoli and Manabe (1990), a number of studies have been performed with both global and regional models, but they have reached conflicting conclusions. Haarsma et al. (1993), for instance, found a significant increase of the number of simulated TCs in greenhouse warming experiments. However, simulations performed with higher-resolution models showed a significant reduction of the global TC activity in a warmer earth (Bengtsson et al. 1996; Sugi et al. 2002; McDonald et al. 2005; Yoshimura et al. 2006; Bengtsson et al. 2007). Royer et al. (1998), on the other hand, found increased (decreased) TC activity in the Northern (Southern) Hemisphere, whereas Chauvin et al. (2006) showed that possible changes in the frequency of TC occurrence in the North Atlantic strongly depend on the characteristics of the sea surface temperature (SST) spatial distribution produced by the scenario simulations.

While the issue of TC frequency response to greenhouse warming remains arguable, some consensus has been achieved about the effects on TC intensity. Several model studies have found that the intensity of simulated TCs tends to increase in a warmer earth (e.g., Walsh and Ryan 2000; Sugi et al. 2002; Knutson and Tuleya 2004; Chauvin et al. 2006; Yoshimura et al. 2006; Oouchi et al. 2006; Bengtsson et al. 2007), consistent with the theoretical findings of Emanuel (1987) and Holland (1997). In particular, these works have shown that in a warmer climate TCs might be characterized by stronger winds and more intense precipitation. These results appear to be robust, because they have been obtained using a variety of models (global and regional), different resolutions, and convective parameterizations. However, it is important to note that most of these studies have been conducted by analyzing experiments performed with atmospheric models forced with prescribed SSTs, and thus the large majority of these experiments do not include air–sea interactions. Moreover, the SST patterns used to force the atmosphere were often based on (generally low resolution) climate scenario simulations performed with other models. This procedure, therefore, may be affected by possible inconsistencies between the simulations from which the SST patterns were taken and the atmospheric simulations used to analyze the TC behavior.

Although the air–sea feedbacks are known to be important for TC intensity (Emanuel 2003), there are only a few analyses of TC response to global warming performed with coupled models, sometimes using limited area models with simplified experimental setting (Knutson et al. 2001). On the other hand, in-depth investigations of TCs and their simulation conducted with fully coupled global models, the same as those used to perform the climate scenarios, would provide further insight into these phenomena and into our ability to reproduce and predict their behavior.

In this study, we document the ability of a high-resolution coupled atmosphere–ocean general circulation model (AOGCM) to simulate tropical cyclone–like vortices and explore how the features of these phenomena are possibly altered by greenhouse warming. The analysis is performed on idealized greenhouse gas forcing scenarios and a simulation of the climate of the twentieth century. The difference with respect to previous works published on the same subject is that we use a fully global coupled model, the atmospheric component of which has the highest horizontal resolution used so far.

In section 2, a description of the model, scenario simulations, and methodological approach used in the present paper is provided. In section 3, we examine the ability of the model to simulate TCs. Section 4 presents an assessment of the possible changes of the TC characteristics as a consequence of global warming. In section 5, the main findings of this work will be discussed, and the summary in section 6 closes the paper.

2. Model, simulations, and methodology

a. The model

The modeling data employed in this work are time series obtained from climate simulations carried out with the SINTEX-G (SXG) AOGCM, which is an evolution of the SINTEX and SINTEX-F models (Gualdi et al. 2003a,b; Guilyardi et al. 2003; Luo et al. 2003; Masson et al. 2005; Behera et al. 2005).

The ocean model component is the reference version 8.2 of the Océan Parallélisé (OPA; Madec et al. 1998) with the ORCA2 global ocean configuration. To avoid the singularity at the North Pole, it has been transferred to two poles located in Asia and North America. The model latitude–longitude resolution is $2° \times 2°$ cosine (latitude), with increased meridional resolutions to 0.5° near the equator. The model has 31 vertical levels, 10 of which lie in the upper 100 m of the ocean.

The model physics includes a free-surface configuration (Roullet and Madec 2000) and the Gent and McWilliams (1990) scheme for isopycnal mixing. The horizontal eddy viscosity coefficient in open oceans varies from 40 000 $m^2 s^{-1}$ in high latitudes to 2000 $m^2 s^{-1}$ at the equator. Vertical eddy diffusivity and viscosity coefficients are calculated from a 1.5-order turbulent closure scheme (Blanke and Delecluse 1993). For more details about the ocean model and its performance, readers are referred to Madec et al. (1998; information also available online at http://www.lodyc.jussieu.fr/opa/).

The evolution of the sea ice is described by the Louvain-La-Neuve sea ice model (LIM; Fichefet and Morales Maqueda 1999), which is a thermodynamic–dynamic snow–sea ice model, with three vertical levels (one for snow and two for ice). The model allows for the presence of leads within the ice pack. Vertical and lateral growth and decay rates of the ice are obtained from prognostic energy budgets at both the bottom and the surface boundaries of the snow–ice cover and in leads. When the snow load is sufficiently large to depress the snow–ice interface under the seawater level, seawater is supposed to infiltrate the entirety of the submerged snow and freeze there, forming a snow–ice cap. For the momentum balance, sea ice is considered as a two-dimensional continuum in dynamical interaction with the atmosphere and ocean. The ice momentum equation is solved on the same horizontal grid as the ocean model. LIM has been thoroughly validated for both Arctic and Antarctic conditions, and has been used in a number of process studies and coupled simulations (Timmermann et al. 2005, and references therein).

TABLE 1. Summary of the climate simulations used in this study.

Climate simulations and scenarios		
Name	Experiment	Length of the analyzed time series
PREIND	Preindustrial GHG concentration	30 yr
20C3M	Twentieth-century GHG concentration + aerosols	30 yr (1970–99)
2CO2	$2 \times$ PREIND CO_2 concentration	30 yr
4CO2	$4 \times$ PREIND CO_2 concentration	30 yr

The atmospheric model component is the latest version of ECHAM4 (Roeckner et al. 1996). We adopted a T106 horizontal resolution, corresponding to a Gaussian grid of about $1.12° \times 1.12°$. In the pantheon of long coupled climate simulations, this is a considerably high horizontal resolution. A hybrid sigma–pressure vertical coordinate is used with 19 vertical levels. The parameterization of convection is based on the mass flux concept (Tiedtke 1989), modified following Nordeng (1994). The Morcrette (1991) radiation scheme is used with the insertion of greenhouse gases (GHGs) and a revised parameterization for the water vapor and the optical properties of clouds. A detailed discussion of the model physics and performances can be found in Roeckner et al. (1996).

The ocean and atmosphere components exchange SST, surface momentum, heat, and water fluxes every 1.5 h. The coupling and the interpolation of the coupling fields is made through the Ocean Atmosphere Sea Ice Soil (OASIS) version 2.4 coupler (Valcke et al. 2000). No flux corrections are applied to the coupled model.

b. The climate scenario simulations

With respect to the previous versions of the SINTEX model, SXG includes a model of the sea ice, which allows the production of fully coupled climate scenario experiments. In this paper, we present results obtained from the analysis of four climate simulations (Table 1).

To assess the capability of the model to reproduce a reasonably realistic TC activity and to evaluate the effectiveness of our TC detection methodology, the tropical cyclone–like vortices produced during the last 30 yr of a twentieth-century simulation have been analyzed and compared with observations. The simulation has been conducted integrating the model with forcing agents, which include greenhouse gases [CO_2, CH_4, N_2O, and chlorofluorocarbons (CFCs)] and sulfate aerosols, as specified in the protocol for the 20C3M experiment defined for the Intergovernmental Panel on Climate Change (IPCC) simulations (more details online at http://www-pcmdi.llnl.gov/ipcc/about_ipcc.php). The integration starts from an equilibrium state obtained from a long coupled simulation of the preindustrial climate, and has been conducted for the entire period of 1870–2000.

Once the skill of the model to reproduce TC-like vortices has been evaluated using the present climate simulation, the possible effects induced by greenhouse global warming on the simulated TCs have been explored using 30 yr of twice-daily data from climate scenario experiments. Specifically, we analyzed a simulation with an atmospheric CO_2 concentration of 287 ppm, corresponding to the preindustrial period (PREIND); a climate simulation with CO_2 concentration doubled with respect to PREIND (2CO2); and a climate simulation with atmospheric CO_2 concentration quadrupled with respect to PREIND (4CO2). The transition between PREIND and 2CO2 and between 2CO2 and 4CO2 has been produced by a 1% yr^{-1} increment of the CO_2 concentration. At the end of the two transition periods, the model has been integrated for 100 yr with constant values of CO_2 concentration, that is, 574 and 1148 ppm, respectively.

A greenhouse warming scenario based on a doubling and quadrupling of atmospheric CO_2 is certainly an idealized experiment and does not represent a realistic forecast of future radiative forcing. The motivation of this choice lies in the fact that a large concentration of atmospheric CO_2 might emphasize the response of simulated TCs to greenhouse warming. Furthermore, the advisability of this kind of idealized experiments in the framework of TC studies has been discussed by Michaels et al. (2005) and Knutson and Tuleya (2005). The possible impact of a doubling of atmospheric CO_2 concentration has also been explored in a number of previous works (e.g., Broccoli and Manabe 1990; Haarsma et al. 1993; Bengtsson et al. 1996; Royer et al. 1998; Sugi et al. 2002; Knutson and Tuleya 2004; McDonald et al. 2005; Yoshimura et al. 2006; Chauvin et al. 2006), but so far no analysis has been performed on the effects of its further increase.

Figure 1 shows the time series of the annual mean values of surface temperature averaged over all latitudes and longitudes, from 1870 to 2000, for the model simulation and observations (Jones et al. 2006). The curves represent the year-to-year deviation of the annual mean with respect to the 1870–90 mean. The observations (dashed curve) show the well-known global warming trend of about 0.6°C over the past century. The model simulation (solid curve) exhibits a similar trend, albeit slightly more pronounced, over the same period. Analogous results are found for the SST field (not shown).

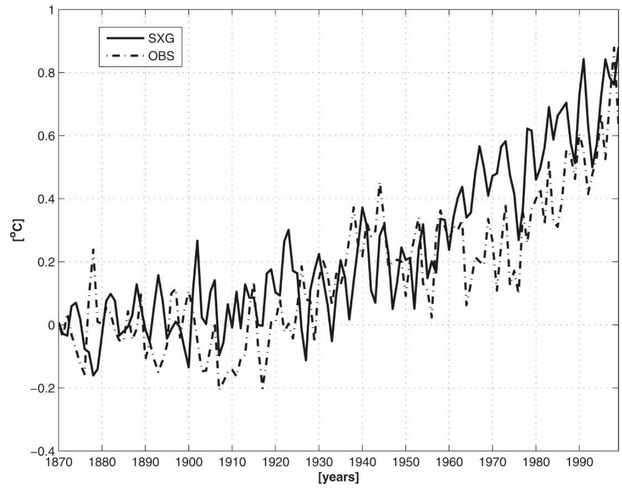

FIG. 1. Time series of the annual mean values of surface temperature averaged over the entire globe. The values plotted are the year-to-year deviation with respect to the 1870–90 mean. Dashed line indicates the observations; solid line indicates the model simulation.

c. Reference data

The simulated TC-like vortices and the main features of their climatology are evaluated by comparing the model results with observational datasets. Specifically, we use data from the National Hurricane Center (NHC) and the U.S. Joint Typhoon Warning Center (JTWC). Furthermore, the capability of the model to reproduce the observed mean climate is assessed using the 40-yr European Centre for Medium-Range Weather Forecasts (ECMWF) Re-Analysis (ERA-40; more information available online at http://www.ecmwf.int/research/era), the observational Hadley Centre Global Sea Ice and Sea Surface Temperature Dataset (HadISST; Rayner et al. 2003), and the observed precipitation dataset produced by Xie and Arkin (1997). For the sake of simplicity, in the rest of the paper we will refer to all of these data as observations.

d. Method of detection of the simulated tropical cyclones

Basically, two methods for detecting TCs have been commonly used in the analysis of general circulation model (GCM) experiment results. The first technique produces an estimate of TC activity based on a genesis parameter computed from seasonal means of large-scale fields (Gray 1979; Royer et al. 1998). This method has been used especially in the analysis of low-resolution model integrations, because it obviates the explicit simulation of individual TCs.

The second method is the location and tracking of individual TCs based on objective criteria for the identification of specific atmospheric conditions that characterize a TC with respect to other atmospheric disturbances. In particular, TCs are identified and tracked as centers of maximum relative vorticity and minimum surface pressure, with a warm core in high levels and maximum wind in the low layers of the atmosphere (Haarsma et al. 1993; Bengtsson et al. 1995; Walsh 1997). In the existing literature, the definition of the criteria, that is, the thresholds and the domain over which they are computed, varies from work to work. A discussion and a short summary for the criteria of objective TC detection in atmospheric analysis and model simulations is given in Walsh (1997) and Chauvin et al. (2006), respectively.

In this study, we use a TC location and tracking method based on the approach defined in Bengtsson et al. (1995) and Walsh (1997). Specifically, we assume that a model TC is active over a certain gridpoint A if the following conditions are satisfied:

1) in A, relative vorticity at 850 hPa is $>3 \times 10^{-5}$ s^{-1};
2) there is a relative minimum surface pressure and wind velocity is >14 m s^{-1} in an area of 2.25° around A;
3) the wind velocity at 850 hPa is $>$ wind velocity at 300 hPa;
4) the sum of temperature anomalies at 700, 500, and 300 hPa is >2°K, where the anomalies are defined as the deviation from a spatial mean computed over an area of 13 grid points in the east–west and 2 grid points in the north–south direction;
5) the temperature anomaly at 300 hPa is greater than the temperature anomaly at 850 hPa;
6) the above conditions persist for a period longer than 1.5 days.

Conditions 3, 4, and 5 distinguish TCs from other low pressure systems, and particularly the extratropical cyclones, which are characterized by strongest winds near the tropopause and a tropospheric cold core. The choice of the parameters in conditions 1–6 are very similar to the values indicated by Bengtsson et al. (1995) and Walsh (1997) and optimize the detection of simulated TCs in our model compared with the observations. The sensitivity of the results to small changes in these parameters has been checked. We found that the number of detected TCs is scarcely sensitive to the threshold values, but exhibits some sensitivity to the size of the areas over which means are computed. For a complete discussion of these criteria and their sensitivity to the parameters used, the reader is referred to Walsh (1997).

3. Simulation of the tropical climate and TC climatology

As a first step, we analyze the results obtained from a simulation of the twentieth century, as described in section 2b, comparing the model results with observations (reanalysis) for the 1970–99 period.

TC occurrence has a pronounced seasonal character, with more intense activity found in the summer hemisphere (Emanuel 2003), namely, in the Northern Hemisphere from June to October (JJASO) and in the Southern Hemisphere from December to April (DJFMA). Therefore, we will focus our attention on the specific seasons (and regions) of intense TC activity.

a. Simulation of mean state and high-frequency variability in the tropics

Figure 2 shows the seasonal means of SST and precipitation as obtained from the observations and model for the extended northern (JJASO) and southern (DJFMA) summers.

In general, the model overestimates the SSTs in the tropical regions for both seasons. The seasonal mean SST averaged over the tropics (23.5°S–23.5°N) is 0.26° and 0.32°C warmer than that observed in JJASO and DJFMA, respectively. The warm bias is visible in both the tropical Indian Ocean and in the Atlantic Ocean, and it is particularly evident in the central-eastern Pacific, south of the equator. In this region, over the warm SSTs, the model also overestimates the rainfall, tending to produce a double ITCZ, which is a common error of most AOGCMs. In the equatorial Pacific, on the other hand, the model cold tongue is clearly too strong and extends too far west. Correspondingly, the simulated precipitation is too weak in the equatorial Pacific, especially west of the date line.

In the tropical Atlantic, the model rainfall is reasonably close to observations in JJASO, whereas during DJFMA it appears to be shifted south (by about 10° latitude), probably as a consequence of the excessively warm SSTs found in the subtropical southern Atlantic, off the Brazilian coast. Interestingly, in the tropical Indian Ocean, the model precipitation is generally weaker than that observed. During the northern summer, the model shows a clear rainfall deficit in the area affected by the Asian summer monsoon, extending from the Bay of Bengal, through Southeast Asia and the South China Sea, and up to the region east of the

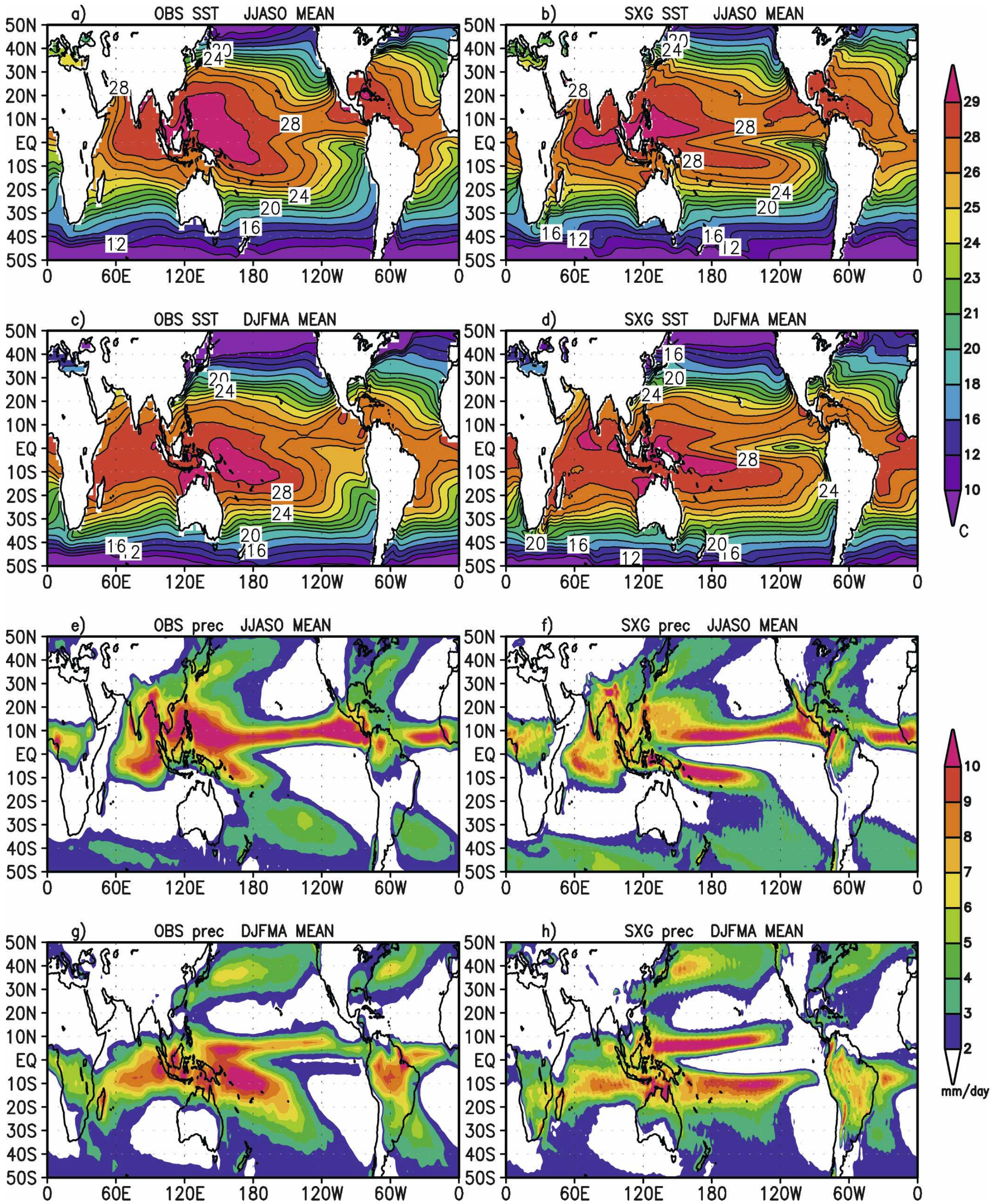

FIG. 2. Seasonal means of SST and precipitation as obtained from the (left) observations and (right) model. (a)–(d) The extended Northern Hemisphere summer means (JJASO) and (e)–(h) the means obtained for the extended Southern Hemisphere summer (DJFMA) are shown. (a), (b), (e), (f) The SST contours are 2°C. (c), (d), (g), (h) The precipitation contours are 1 mm day^{-1}. Rainfall values lower than 2 mm day^{-1} are not plotted.

Philippines archipelago. Simulated precipitation also appears to be too weak over the eastern equatorial Indian Ocean, whereas it tends to be too intense in the western part of the basin, between the equator and 10°S. During the northern winter (Figs. 2g,h) model rainfall is too weak over the eastern Indian Ocean and the Indonesian region.

A first estimate of the variability of the convective

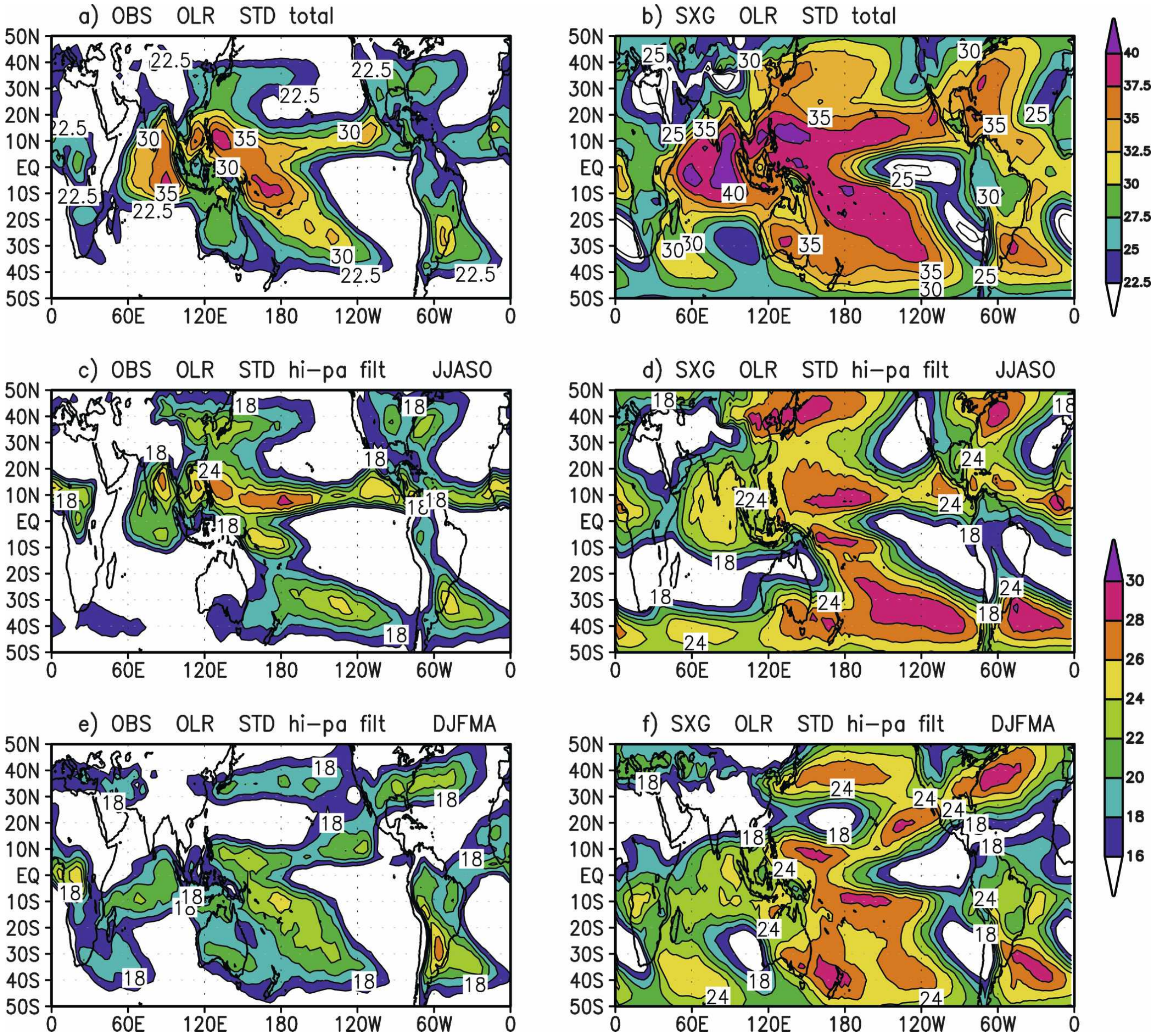

FIG. 3. Standard deviation (STD) of the OLR obtained from daily anomalies for the period 1979–2000 for the (left) observations and (right) model. The STD of the (a), (b) total anomalies and (c), (d) high-pass filtered anomalies for the northern summer (JJASO). (bottom) The results from the high-pass-filtered anomalies for the southern summer (DJFMA). The filtered anomalies have been obtained by applying a Fourier filter to suppress signals with periods longer than 10 days. The contour line interval is 2.5 W m^{-2} for the STD of the total field (first row), whereas it is 2 W m^{-2} for the STD of the filtered anomalies (second and third rows).

activity can be obtained from the standard deviation of the outgoing longwave radiation (OLR). Figure 3 shows the standard deviation of OLR, for observations (left column) and model simulation (right column), as obtained from daily anomalies. In observations, the pattern of total variability (Fig. 3a) shows maxima over the eastern Indian Ocean, from the equatorial region to the Bay of Bengal and over the western Pacific, extending from the Philippines southeastward along the southern Pacific convergence zone (SPCZ) and eastward along the ITCZ. Secondary maxima are found over tropical West Africa (the region of the African monsoon) and in the extratropics over South and North America, along the western Atlantic coast. The model (Fig. 3b) exhibits some tendency to overestimate the OLR variability, but the location of the model maxima is mostly consistent with observations. In the tropics, the excess of simulated convective variability is particularly noticeable in the central Pacific, south of the equator and east of the date line, in the western Atlantic, and in the western Indian Ocean.

The standard deviations of the daily OLR anomalies shown in Fig. 3 (upper panels) give an estimate of the convective variability integrated over all time scales, but here we are specifically interested in phenomena that have relatively short time scales; thus, the OLR anomalies have been high-pass filtered, removing signals with periods longer than 10 days, before computing

TABLE 2. Total number of tropical cyclones found in the observations and in the twentieth-century model simulation during the 1970–99 period.

	No. of TCs, 1970–99	
	OBS	SXG 20C3M
Tot	2813	1986
Mean	93.8	66.2
STD	10.9	9.2

the standard deviations. The patterns of the high-frequency variability are shown in Fig. 3 (middle and lower panels) for the northern and southern summers, respectively, for both the model and observations. In this case too, the model exhibits some ability to capture the distribution of convective variability. In particular, during the northern summer the simulated high-frequency convective variability appears to be quite realistic, with maxima located in the western tropical Pacific, along the Pacific and Atlantic ITCZ and along the storm tracks in the winter hemisphere. During the southern summer the model tends to overestimate the variability, especially in the subtropical central Pacific and in the midlatitude northern Pacific. The model tendency to produce an excess of high-frequency variability in the tropics is also visible when one examines the dynamical fields, such as the low-level meridional wind velocity, for example (not shown).

b. Simulation of tropical cyclones

In this section we analyze the ability of the model to simulate tropical cyclones–like vortices (which we shall refer to simply as TCs), following the methodology discussed in section 2d. As a first step, we compare the total number of TCs per year detected in the model simulation and in the observations over the 1970–99 period (Table 2). In general, the number of simulated TCs per year is almost 30% lower than the number detected in the observations, whereas its standard deviation is quite well captured by the model. Noteworthy, if we normalize the standard deviations with the mean values, then the variability found in the model is slightly higher (16%) than the observed one.

The geographical distribution of the TC formation positions is shown in Fig. 4. In the observations (Fig. 4a) there are four distinct regions of TC formation in the tropics of the Northern Hemisphere—northern Indian Ocean (NI), western North Pacific (WNP), eastern North Pacific (ENP), and North Atlantic (ATL) and three regions in the Southern Hemisphere—southern

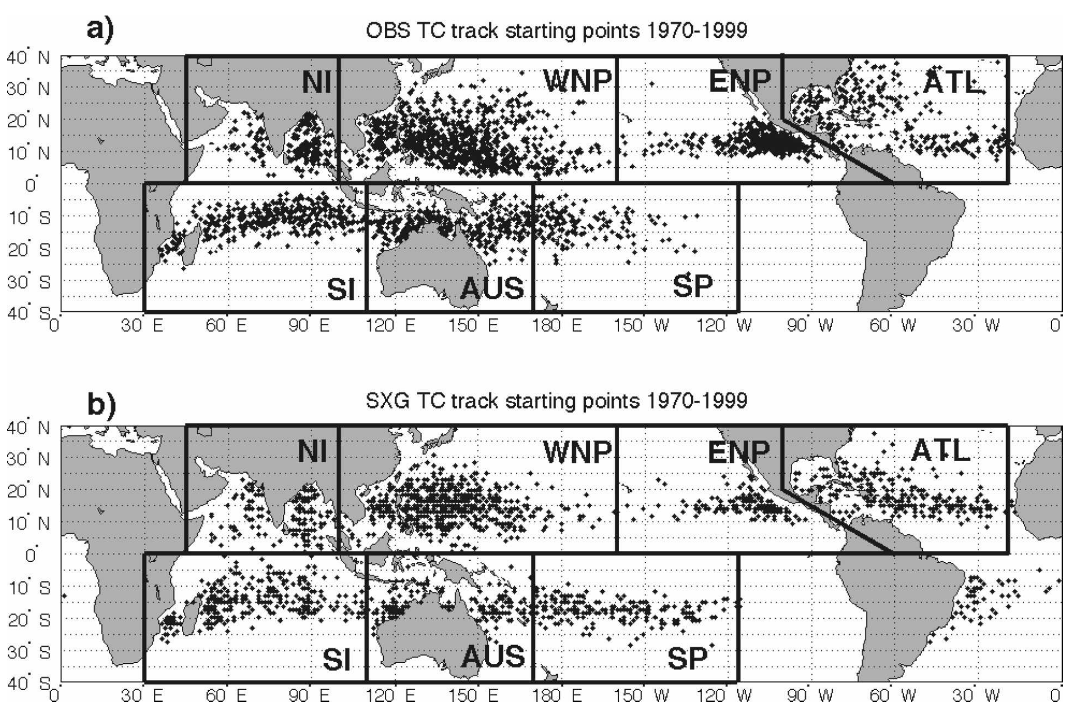

FIG. 4. Distribution of the TC track starting points for the period 1970–99 for the (a) observations and (b) model. Each point corresponds to the geographical location of a TC at the time of its first detection. Following Camargo et al. (2004) seven regions of TC genesis have been defined. In the pictures these regions are delimited by thick black lines.

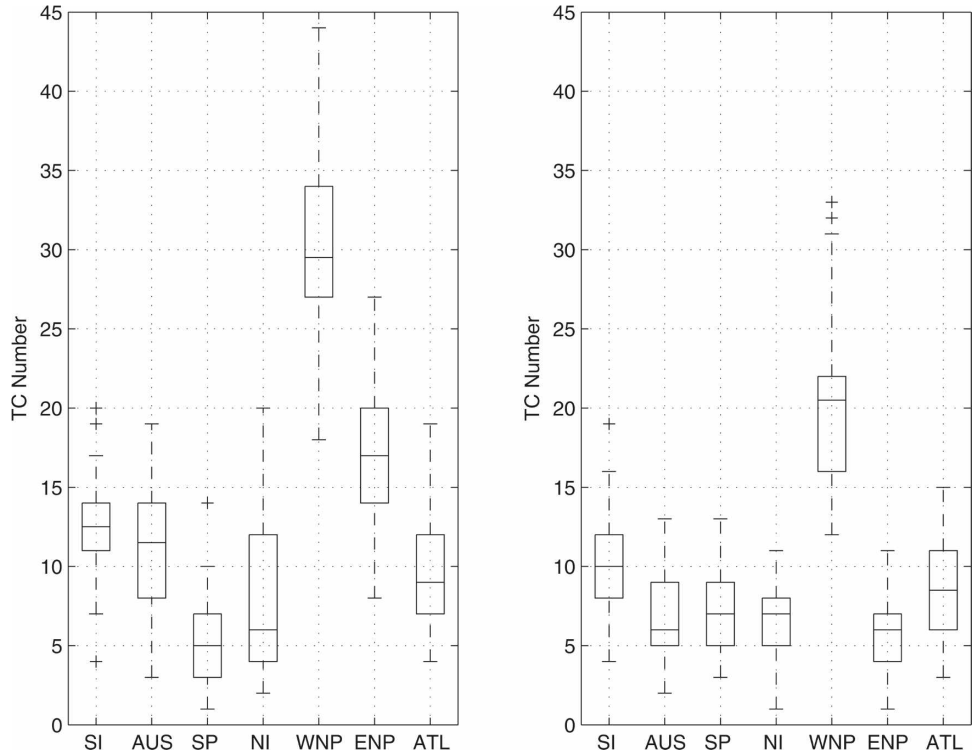

FIG. 5. Box plots of the number of TCs per year for the (left) observations and (right) model simulation. The number of TCs (y axis) is plotted for each area of TC genesis (x axis) defined in Fig. 4. In a box plot, the box represents the interquartile (IQR) and contains the 50% of the data; the upper edge of the box represents the 75th percentile [upper quartile (UQ)], while the lower edge is the 25th percentile [lower quartile (LQ)]. The horizontal lines within the box are the median. The vertical dashed lines indicate the range of the nonoutliers. The values indicated with the crosses are the outliers, i.e., values that are either larger than UQ + 1.5 IQR or smaller than LQ − 1.5 IQR.

Indian Ocean (SI), the ocean north of Australia (AUS), and the southern Pacific (SP). Based on these regions of TC genesis, and following Camargo et al. (2004), we define seven basins (see the boxes in Fig. 4) that will be used to delimit the different areas of TC activity.

The model (Fig. 4a) reproduces the patterns of TC genesis well, especially in the Northern Hemisphere. The major difference compared to the observations occurs in the southern Atlantic, where the model generates some TC, though no TCs have been observed in this region during the period considered (1970–99). This model error might be related to the excessively warm SSTs and intense convective activity found in this region (Fig. 2). However, it is noteworthy that in March 2004 the first ever observed TC in South America, named Catarina, hit the Brazilian coast (Pezza and Simmonds 2005).

A comparison with the results obtained with atmospheric GCMs forced with observed prescribed SSTs (Camargo et al. 2004, their Fig. 2) shows a substantial improvement in the patterns of TC genesis obtained with the coupled simulation. Interestingly, the comparison is made more valid by the fact that one of the atmospheric models used in Camargo et al. (ECHAM4) is basically the same as the one that we use as the atmospheric component in our coupled model. An important difference, however, is the horizontal resolution, which is T42 in Camargo et al. and T106 in our case. The enhanced model resolution might explain some of the improvements we find with our model, such as the increased global number of TCs, accompanied by a significant reduction of the number of TCs near the equator, which is a rather unrealistic feature (e.g., Camargo et al. 2004; Oouchi et al. 2006).

In Fig. 5, we show the box plots representing the mean number of TCs per year for each area both for the observations (left panel) and the model (right panel). The figure confirms that in the simulation there is a lower number of TCs, especially in the tropical North Pacific (WNP and ENP). However, in general the difference with the observations is relatively small, and, for each area, the model simulates a fairly realistic mean year-to-year variability (see also STD in Table 2). More importantly, the simulation appears to capture

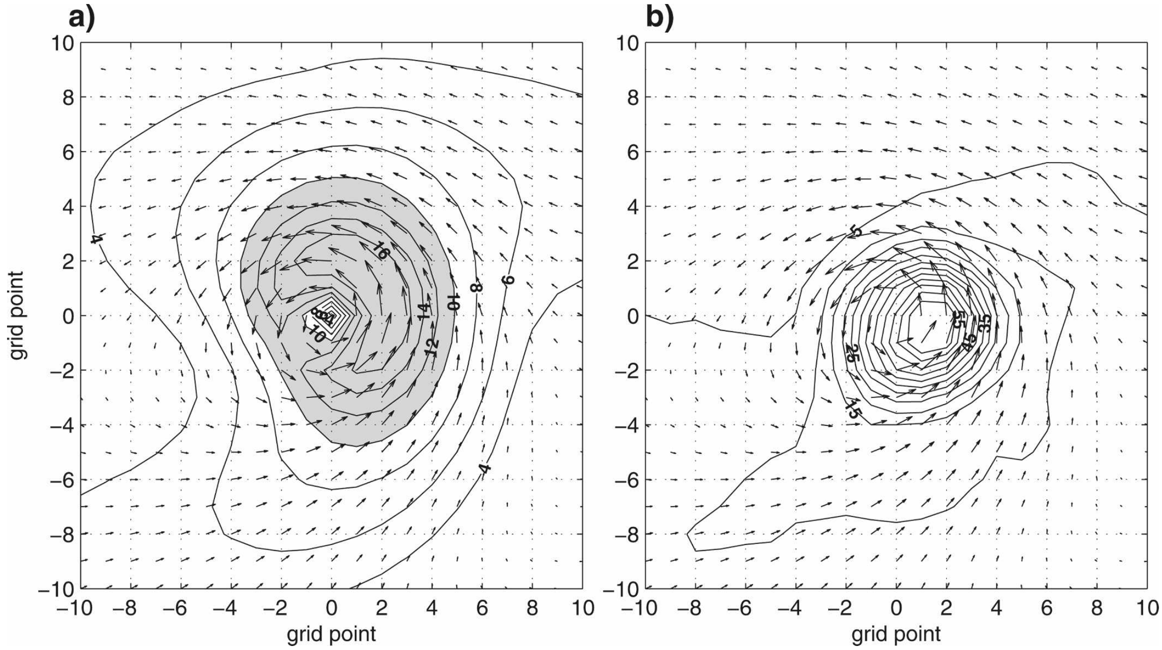

FIG. 6. Composite patterns of (a) 850-hPa wind and (b) total precipitation associated with the simulated TCs. The composites have been computed by averaging the fields of the 100 most intense (in terms of precipitation) model TCs in the Northern Hemisphere. The fields have been averaged over the period of occurrence of the TCs and over the 100 events. The mean fields have been computed over a spatial domain centered in the core of the cyclone and extending 10° each side. In (a) the direction of 850-hPa wind (arrows) is plotted along with the intensity of the wind (contour). The contour interval is 2 m s^{-1}. Contours larger than 10 m s^{-1} are shaded. In (b) the 850-hPa wind (arrows) along with the total precipitation rate is shown. The contour interval is 5 mm day^{-1}.

the basic features of the TC distribution over the different areas. Specifically, the region with the highest mean number of TCs per year is the WNP both in the model and observations. The mean number of TCs in the NI and ATL are also reproduced well, whereas the TC activity in the ENP is clearly underestimated.

The results shown in Figs. 2–5 indicate that the model reproduces a quite realistic tropical mean state (at least in terms of SST and precipitation) and number of simulated TC-like vortices. Furthermore, the geographic distribution of TCs appears to be in good agreement with the observations.

To have a closer look at the structure of the model TCs, Fig. 6 depicts the composite patterns of precipitation and low-level wind field obtained from the 100 most intense simulated TCs in the Northern Hemisphere. The composites were calculated by averaging the fields over the period of occurrence of the TCs and over the 100 events. The means have been computed for a domain centered on the core of the cyclones and extending 10° each side.

These patterns indicate that the model simulates TCs with a somewhat realistic structures. When averaged over the 100 events and their lifetimes, the mean TC has intense mean precipitation and surface winds that extend for about 300–400 km from the center ("eye") of the cyclone. The amplitude of the fields is substantially smaller than that observed, but is consistent with the results obtained from high-resolution atmospheric GCM experiments (e.g., Bengtsson et al. 1995; Chauvin et al. 2006). In agreement with observational studies (e.g., Frank 1977; Gray 1979; Willoughby et al. 1982), the strongest wind velocities are located to the right-front sector of the core, though the maxima in the model is much too far away from the eye. This model error is most likely due to the model resolution, which does not allow resolution of the fine and tight structures observed in "real" TCs, as suggested in McDonald et al. (2005) and Chauvin et al. (2006), and shown in Bengtsson et al. (2007). For the same reason, the minimum surface pressure at the center of the storm (not shown) tends to be rather high (990 hPa) and the simulated TC does not exhibits the eye in the precipitation, though in general the rainfall pattern is reasonably realistic.

An important feature of the observed TCs is their marked seasonal character (Emanuel 2003). Figure 7 shows the seasonality of TC occurrence for both observations and model simulations in the Northern and Southern Hemispheres and for specific regions of activity described in Fig. 4. In general the model repro-

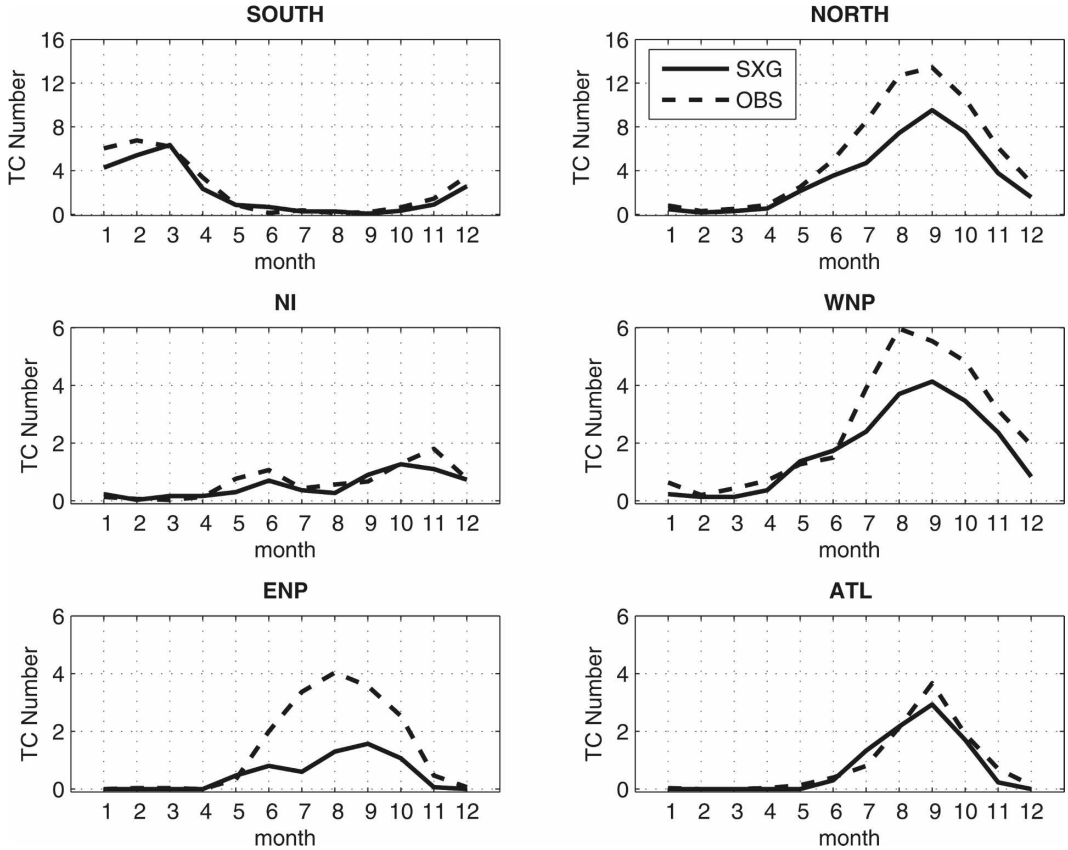

FIG. 7. Seasonal modulation of the TC occurrence for the observations (dashed lines) and model simulation (solid lines) and for different region of the tropics. (top) Tropical region of the (left) Southern and (right) Northern Hemisphere. (middle and bottom) Northern Indian Ocean, western tropical Pacific, eastern tropical Pacific, and tropical Atlantic.

duces the seasonal behavior of TCs well, especially in the Southern Hemisphere and the northern Indian and Atlantic Oceans. In the Northern Hemisphere, and particularly in the northwest and northeast Pacific, the annual phase of the TC activity is captured but the amplitude is much smaller, consistent with the reduced number of simulated TCs previously discussed.

In addition to the seasonal modulation, the TC activity exhibits a rather strong year-to-year variability. As has been shown in a number of studies (Gray 1984; Chan 2000; Chia and Ropelewski 2002; Frank and Young 2007; among others), this interannual variability has a strong link with ENSO. Changes in the SST distribution in the tropical Pacific and the associated changes in the large-scale circulation, in fact, appear to have a strong impact on the number of TCs that occur in different regions of the globe. The relationship between ENSO and TC activity is different depending on the region considered. Frank and Young (2007) have shown that the number of observed TCs and the Niño-3 (5°N–5°S, 150°–90°W) ENSO index are negatively correlated in the North Atlantic ($r = -0.55$), whereas they appear to be positively correlated in the northeast Pacific ($r = 0.38$) and Indian Ocean ($r = 0.24$).

Figure 8 shows the interannual variation of the number of TCs in the North Atlantic, northeast Pacific, and southern Indian Ocean (solid curves), along with the Niño-3 SSTA index (dotted curves). Here, the value of the Niño-3 index is computed for the season of maximum TC activity, that is, JJASO for the Northern Hemisphere and DJFMA for the Southern Hemisphere. The curves shown in Fig. 8 indicate that the model simulates a fairly realistic interannual modulation of the number of TCs and that this interannual variability is correlated with ENSO similarly to what is found in the observations.

All of these results indicate that the model simulates intense convective disturbances with characteristics similar to the basic features of observed TCs, which is reassuring with regard to its suitability for investigating how climate change might impact on the TC activity, which will be the subject of the following section.

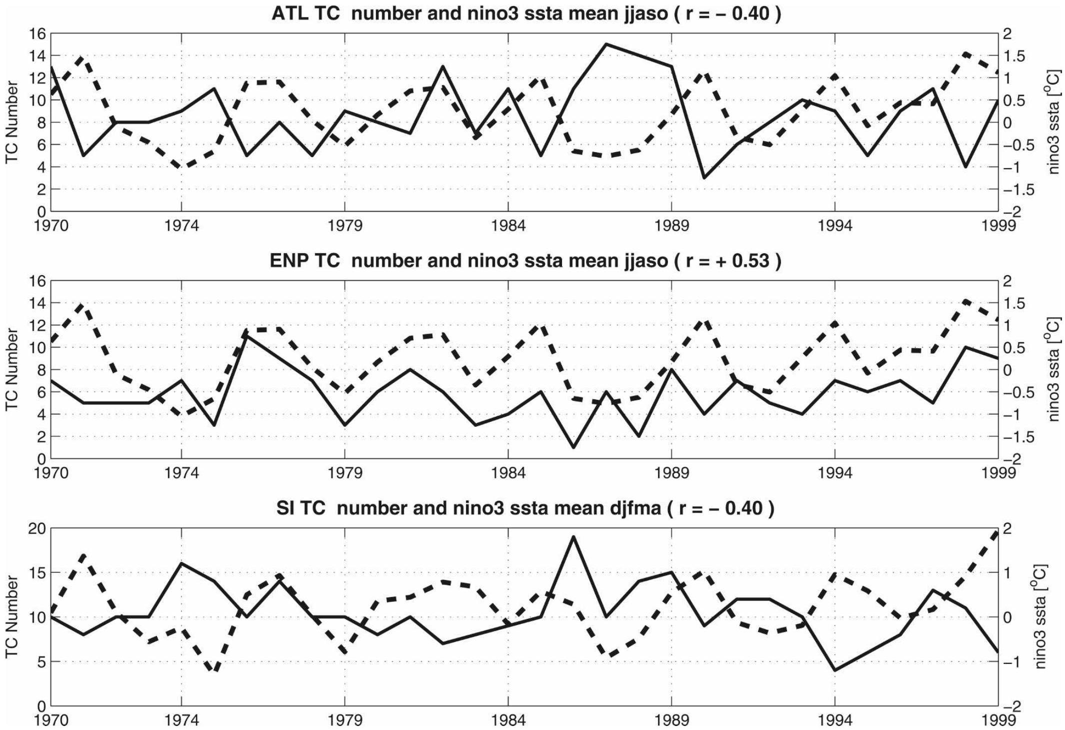

FIG. 8. Time series of the number of TCs along with the Niño-3 index for different regions of the tropics. The solid lines show the interannual variation of the number of simulated TCs in the (top) northern tropical Atlantic, (middle) northern tropical eastern Pacific, and (bottom) southern Indian Ocean. The dashed lines show the value of Niño-3 SSTA index defined as the average of the SST anomaly over the Niño-3 region (5°S–5°N, 150°–90°W). The values of the Niño-3 index plotted in the ATL and ENP case have been obtained for JJASO, whereas for the SI case it has been computed for DJFMA. The value of the correlation between the two curves (*r*) is also shown.

4. Impacts of global warming on the tropical climate and TC climatology

Possible changes in the basic features of the tropical mean climate and of the simulated tropical cyclones resulting from greenhouse global warming are investigated using the climate scenario experiments PREIND, 2CO2, and 4CO2 described in section 2b. Figure 9 shows the time series of the annual mean values of surface temperature averaged over all latitudes and longitudes for the scenarios, along with the 20C3M simulation. The curves represent the year-to-year deviation of the annual mean with respect to the 1840–70 mean, that is, the mean of the last 30 yr of PREIND.

In the PREIND experiment (Fig. 9, dashed curve), the series of the mean surface temperature exhibits a slight negative trend of about 0.024°C decade^{-1}. This drift is very likely due to the fact that the model is still adjusting toward its preindustrial climate equilibrium. The trend is very small, especially during the period used for our analysis (i.e., the last 30 yr of the PREIND time series), where its amplitude is of about -0.009°C decade^{-1}. Thus, it is unlikely that it can have a significant impact on our results.

As already discussed in section 2b, during the twentieth century the model simulates a reasonably realistic global warming (dashed–dotted curve), which is albeit slightly more pronounced than that observed. The 1% yr^{-1} CO_2 increment produces a much larger impact on the global temperature. In the CO_2 experiment (solid curve), during the stabilization period at $2 \times CO_2$, the global mean temperature at the earth surface is about 2°C warmer than in the preindustrial simulation. A warming larger than 4°C is obtained when the CO_2 is quadrupled (4CO2; dotted curve).

a. Changes in the tropical mean state

The impact of the increased atmospheric CO_2 on the mean state of the tropics is shown in Fig. 10. Here the difference between 2CO2 and PREIND (2CO2 − PREIND) and 4CO2 and PREIND (4CO2 − PREIND) seasonal means of SST and precipitation are shown. Figures 10a,b,e,f indicate that the overall warming of the tropical SST is characterized by regional patterns. During both JJASO and DJFMA, in fact, the warming is more visible in the western part of the Indian Ocean, in the equatorial Pacific, and along the coast of South

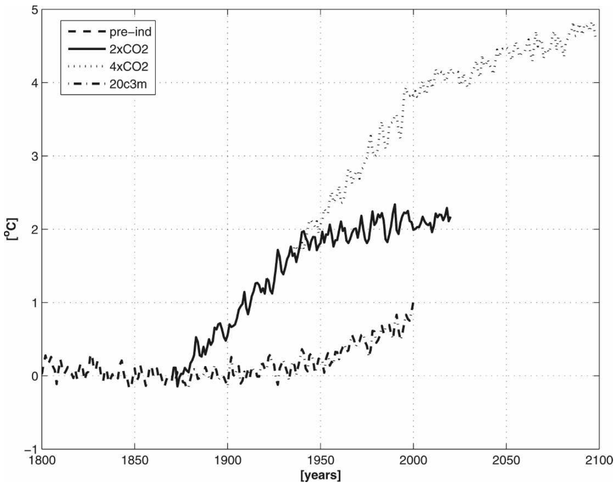

FIG. 9. Time series of the annual mean values of surface temperature averaged over the entire globe for PREIND (dashed curve), 20C3M (dashed and dotted curve), 2CO2 (solid line), and 4CO2 (dotted curve). The values plotted are the year-to-year deviation with respect to the 1870–90 mean.

America, whereas a weaker warming is found in the eastern tropical Indian Ocean and eastern subtropical Pacific. In the tropical Pacific the warming patterns resemble El Niño anomalies. Interestingly, these patterns are similar for the 2CO2 − PREIND and 4CO2 − PREIND cases, albeit with different amplitudes.

Similar characteristics are exhibited by the patterns of difference between the PREIND, 2CO2, and 4CO2 precipitation (Figs. 10c,d,g,h). In particular, the increased CO_2 induces a remarkable enhancement of precipitation along the ITCZ, from the Indian Ocean, through the Pacific, to the Atlantic, during JJASO. Interestingly the increase of rainfall is confined to a relatively narrow region, very close to the equator. In the same season, areas of reduced rainfall are located in the southeastern tropical Indian Ocean and south-central Pacific. During DJFMA, increased precipitation is found south of the equator, along the southern branch of the double ITCZ simulated by the model and discussed in section 3a, whereas regions of decreased rainfall are found in the subtropics of both the summer and winter hemispheres. In this case too, the patterns of precipitation difference 2CO2 − PREIND and 4CO2 − PREIND exhibit very similar spatial features but different amplitudes.

Table 3 shows the changes in mean temperature, mean precipitation, and mean convective precipitation over the entire globe and over the tropics for the three experiments. Here, the convective precipitation is the precipitation associated with convective processes and produced by the convective parameterization scheme. Interestingly, while a substantial rise in mean surface temperature and mean total precipitation are found when the CO_2 is increased, a completely different behavior is found for the convective precipitation. The latter, in fact, shows a significant reduction when the atmospheric CO_2 concentration has doubled and quadrupled, especially in the tropical region. In a recent work performed with a simplified model, Held et al. (2007) found similar changes in the partition of the tropical precipitation between being large scale and convective when the SSTs are increased.

Figure 11 shows the changes in high-frequency convective variability induced by the CO_2 forcing in terms of the difference in standard deviation of high-pass-filtered OLR anomalies. For the sake of brevity, only the difference between 4CO2 and PREIND is considered (2CO2 − PREIND produces very similar patterns, with a smaller amplitude). Over most of the tropical belt the sign of the difference is negative, indicating a tendency of the model to attenuate the high-frequency convective variability when the atmospheric CO_2 is increased. Only over the equatorial Pacific, between about 5°N and 5°S, is there a clear sign of enhanced variability.

These results appear to suggest that by increasing the concentration of CO_2 in the atmosphere of the model, general warming of the earth's surface is accompanied by a reduction of (deep) convective activity in the tropics. The weaker convective activity, in turn, might be due to an enhancement of vertical stability of the atmosphere. This point will be examined in more detail in section 5.

b. *Changes in the simulated tropical cyclones*

Let us now consider what happens to the simulated TCs as a consequence of greenhouse global warming. Table 4 shows the total number of TCs and TC days (upper row), the annual mean number of TCs and TC days (middle row), and their standard deviations (lower row) for the PREIND, 2CO2, and 4CO2 experiments. The method for detecting the TCs in these experiments is the same as that used for the twentieth century and discussed in section 2d. In this case as well we checked the sensitivity of the results to changes in the parameters used in the tracking procedure. In particular, we checked whether the results obtained from the 2CO2 and 4CO2 simulations might be affected by the choice of the vertical levels used to detect the warm core (700, 500, and 300 hPa). The analysis indicated that the results shown in Table 4 are scarcely sensitive to small changes in the criteria we adopted.

The results illustrated in Table 4 suggest that the total number and the annual mean number of TCs and TC days appear to be substantially reduced with an

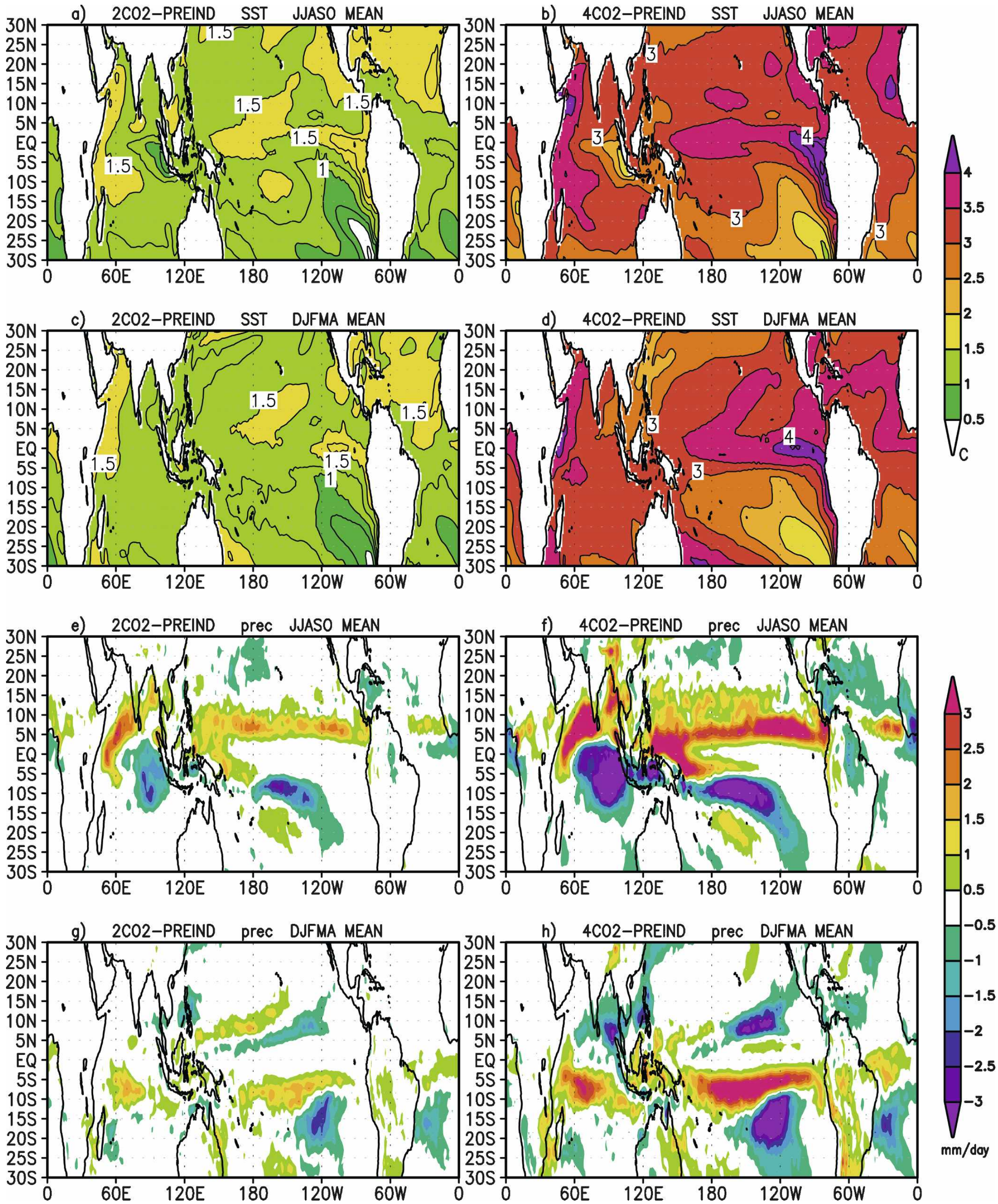

FIG. 10. Differences between the seasonal mean SST and precipitation obtained from (left) 2CO2 and PREIND and (right) 4CO2 and PREIND. (a), (b), (e), (f) The differences in mean SST; contour interval is 0.5°C; (c), (d), (g), (h) the differences in mean precipitation, with a contour interval of 0.5 mm day^{-1}.

increased concentration of atmospheric CO_2, whereas their interannual variability does not show significant changes. The average duration of TC (2.7 days for PREIND and 4CO2, and 2.8 days for 2CO2) does not exhibit substantial variations either. Our simulations, therefore, indicate that increased CO_2 leads to a reduction of the TC activity, both in terms of number of TCs and number of TC days. These results are consistent with previous findings (e.g., Bengtsson et al. 1996; Sugi et al. 2002; McDonald et al. 2005; Yoshimura et al.

TABLE 3. Global average and tropical average (23.5°S–23.5°N) of mean surface temperature, mean total precipitation, and mean convective precipitation. The mean have been computed over the 30-yr periods considered in the study. Values in parentheses are the differences (absolute values for temperature and percentage for precipitation) with respect to the PREIND case.

	PREIND	2CO2	4CO2
$T_{\text{global mean}}$ (K)	288.37	290.377 (+2.01)	292.72 (+4.36)
T_{Tropics} (K)	298.72	300.286 (+1.57)	302.41 (+3.69)
$\text{Prec}_{\text{global mean}}$ (mm day^{-1})	2.757	2.809 (+1.89%)	2.852 (+3.45%)
$\text{Prec}_{\text{Tropics}}$ (mm day^{-1})	3.317	3.353 (+1.09%)	3.354 (+1.12%)
$\text{ConvPrec}_{\text{global mean}}$ (mm day^{-1})	1.209	1.164 (−3.72%)	1.106 (−8.52%)
$\text{ConvPrec}_{\text{Tropics}}$ (mm day^{-1})	2.117	2.008 (−5.15%)	1.884 (−11.01%)

2006), and for the first time they have been obtained using climate scenario simulations performed with a state-of-the-art fully coupled high-resolution GCM.

The box plots shown in Fig. 12 represent the mean number of TCs per year for each activity area and for the three experiments. The reduction of the number of TCs is visible in all of the regions, although it appears to be particularly evident in the WNP and ATL areas. Interestingly, TC activity also appears to be drastically reduced in the tropical South Atlantic (SATL).

Observational studies have hypothesized the existence of an Atlantic Multidecadal Oscillation (AMO; e.g., Delworth and Mann 2000), which by varying the Atlantic SST might influence the low-frequency variation of TC activity in this region (Goldenberg et al. 2001). If the model produces an AMO-like variation of the SSTs and a consequent modulation of the Atlantic TC frequency, then the changes found in the TC number and shown in Fig. 12 could be due to a low-frequency "natural" oscillation of the storm activity. Figure 13 shows the time series of the number of TCs in the North Atlantic for 90 yr of the PREIND climate simulation (dashed line) and the 4CO2 experiment (dotted curve). The curves have been smoothed with a 10-yr running mean. In the PREIND case, the series shows a pronounced decadal variation of the TC number, which is apparently much more pronounced than that in the 4CO2 case. However, the amplitude of the oscillation is much smaller than the differences between 4CO2 and PREIND, and during the phases of lower TC activity, the number of storms in PREIND is higher than that in 4CO2. Therefore, even considering the model "natural" (internal) low-frequency modulation of the TC activity, the number of TCs in the PREIND climate is systematically larger than in the 4CO2 case. This result suggests that the marked reduction of Atlantic TC number in the 4CO2 experiment is most likely ascribable to the greenhouse warming.

Generally, it is accepted that TCs tend to develop over oceanic warm waters. Specifically, climatological studies (e.g., Palmen 1948) indicate that the SST has to be warmer than about 26°C. The overall warming of the SST (shown in Fig. 10) implies a poleward migration of the 26°C isotherm, and one might therefore expect to find a poleward extension of TC activity in a warmer climate.

Figure 14 shows the zonal average of the total number of simulated TCs (left panels, dashed lines) and the

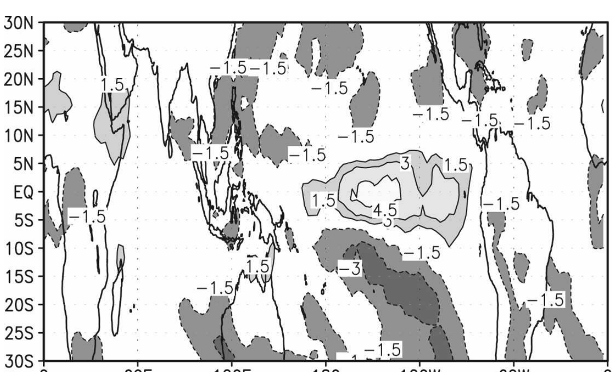

FIG. 11. Difference between the standard deviation of the high-pass-filtered OLR anomalies obtained from the 4CO2 and the PRIND experiments. The OLR anomalies have been filtered as explained for Fig. 3. Contour interval is 1.5 W m^{-2}. Dashed lines and dark shading indicate negative values of the difference. Solid line and light shading indicate positive values of the difference.

TABLE 4. (first row) Total number of TCs and total number of TC days found in the PREIND, 2CO2, and 4CO2 experiments. In all of the experiments a 30-yr period is considered. (middle row) the mean number of TCs and TC days per year; (bottom row) the year-to-year standard deviation of the annual number of TCs and TC days. The average duration of the TCs, defined as the ratio between number of TC days and number of TCs, is 2.7 days for PREIND, 2.8 for 2CO2, and 2.7 for 4CO2.

	Number of tropical cyclones			Number of tropical cyclone days		
	PREIND	2CO2	4CO2	PREIND	2CO2	4CO2
Tot	2196	1839	1229	5941	5085	3313
Mean	73.2	61.3	41.0	198.0	169.5	110.4
STD	6.8	8.3	7.6	22.5	24.0	23.3

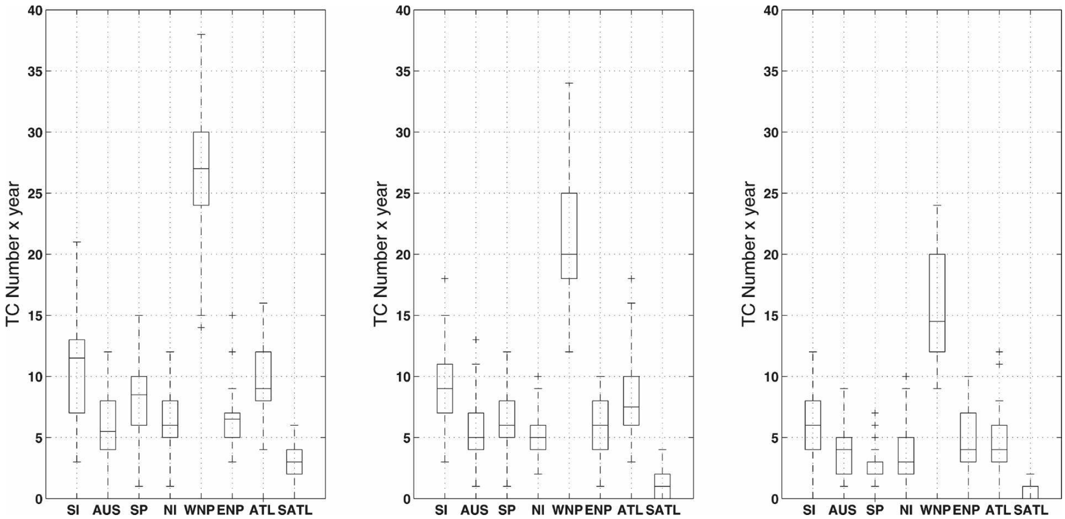

FIG. 12. Box plot of the annual number of TCs in the areas defined in Fig. 4 and for the SATL region: (left) PREIND, (middle) 2CO2, and (right) 4CO2 experiments.

number of TC days (right panels, dashed lines) along with the zonal mean SST (solid lines) for the three experiments: PREIND (upper panels), 2CO2 (middle panels), and 4CO2 (lower panels). In the PREIND case the zonal mean SST threshold for TC occurrence appears to be between 25° and 26°C. The maximum number of TCs and TC days occurs slightly equatorward of 20° latitude in both hemispheres.

Increasing the atmospheric CO_2 (middle and lower panels) the 26°C isotherm migrates poleward, on average, by almost 10° of latitude, but the latitudinal distribution of the number of TCs and TC days does not appear to be substantially changed. The maxima of TC occurrence, although reduced, still appears to be confined equatorward of 20° latitude, and the number of TC days tends to vanish poleward of 30° latitude. On the other hand, the zonal mean SST threshold for TC occurrence increases to about 28°C and to almost 30°C for the 2CO2 and 4CO2 cases, respectively. These results, in agreement with previous works (e.g., Haarsma et al. 1993; Henderson-Sellers et al. 1998) suggest that the poleward migration of warm SSTs caused by greenhouse global warming does not imply an extension of the regions of cyclogenesis or TC activities toward the middle latitudes. Similar findings for the relationship between SSTs and convective precipitation have been indicated by Dutton et al. (2000).

To assess possible modifications in the strength of the simulated TCs, we have analyzed the changes in intensity of low-level winds, minimum surface pressure, and precipitation associated with the model TCs. The intensity of the TC low-level wind has been analyzed using the power dissipation index (PDI) proposed by Emanuel (2005), whereas as an index of intensity of TC precipitation we consider the rainfall averaged over a 4 × 4 gridpoint area around the center of the cyclone and throughout the duration of the event.

When the probability distribution function (pdf) of the PDI for the three experiments is computed and plotted (Fig. 15, upper panel), the curves do not show significant differences. Similar results are obtained from the pdf of the lowest TC minimum surface pressure (lower panel). Thus, in terms of strength of the near-surface wind, the changes in atmospheric CO_2 do not appear to affect the intensity of the simulated TCs. Simulations performed with very high-resolution atmospheric models, on the other hand, showed that in a

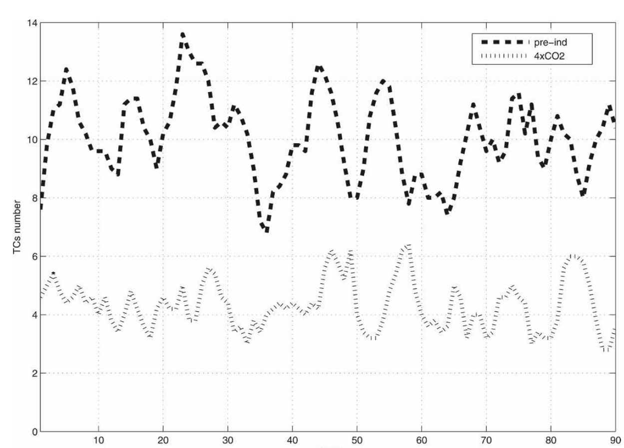

FIG. 13. Time series of TC numbers in the North Atlantic for 90 yr of the PREIND simulation (dashed line) and 90 yr of the 4CO2 experiment (dotted curve). The curves have been smoothed with a 10-yr running mean.

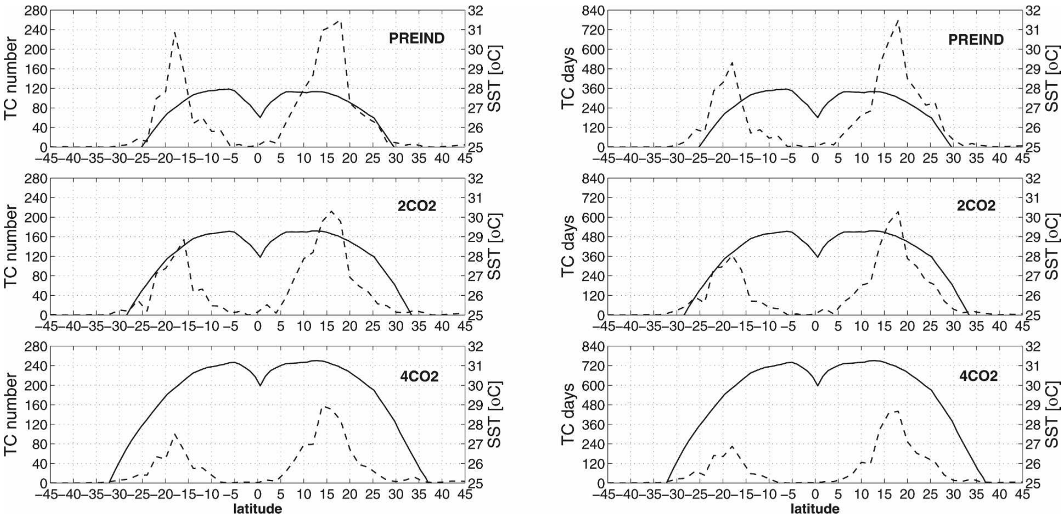

FIG. 14. Latitudinal distribution of the total number of (left) simulated TCs and (right) TC days, and zonal mean value of SST for the (top) PREIND, (middle) 2CO2, and (bottom) 4CO2 experiments. The x axis is the latitude. The y axis is the (left) number of TCs and TC days and (right) the SST value. The dashed curves show the meridional distribution of the total number of TCs and TC days, with maxima centered between 15° and 20° latitude in both hemispheres. The solid curves show the distribution of the zonal mean SST. The two curves indicate, for each latitude, the number of TCs and the number of TC days and the corresponding values of SST.

warmer climate the pdf of TC intensity shifts to higher values, with a decrease of the weaker cyclones and an increment of the most intense ones (Knutson and Tuleya 2004; Oouchi et al. 2006; Bengtsson et al. 2007). In particular, Bengtsson et al. (2007) has shown that the shift becomes more evident, increasing the model horizontal resolution. We think that this shift does not occur in our simulations because of the deficiencies that our model appears to have in simulating intense events. It is likely, in fact, that the model produces the most intense TCs that it is capable of simulating even in the PREIND climate, at least in terms of surface wind and minimum surface pressure. Therefore, the apparent lack of impact of the global warming on the simulated PDI and surface pressure might actually be due to the difficulties of the model in representing TC intensity, which in turn are probably caused by insufficient horizontal resolution.

Different findings are obtained when we use the precipitation field to quantify the intensity of the model TCs. Figure 16 shows the pdf of precipitation (total, convective, and nonconvective) associated with a model TC for four different regions of activity and for the three experiments. In all of the cases, the maximum of pdf appears to shift to higher values of rainfall when the CO_2 increases, indicating that in general in a warmer climate the TCs tend to be accompanied by more intense precipitation.

To confirm these findings further, in Fig. 17 the composite of TC precipitation are shown. The composite

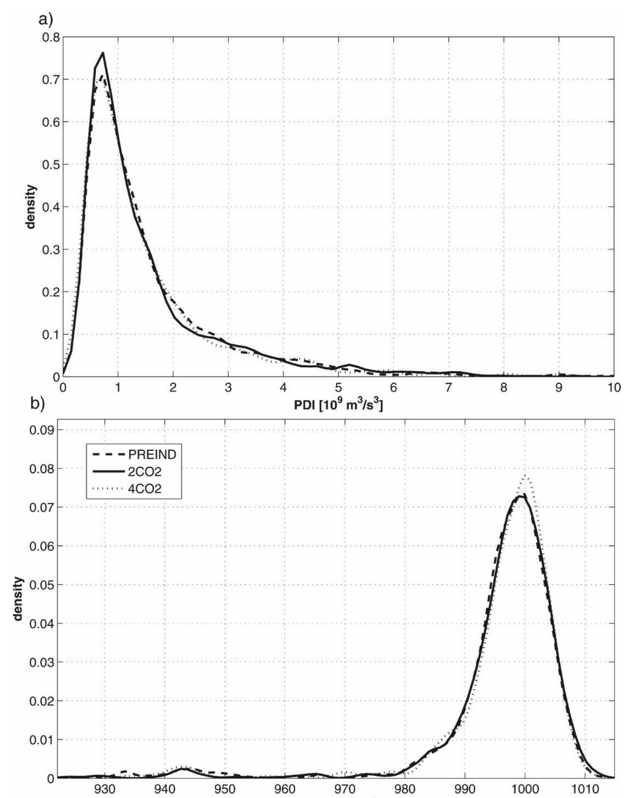

FIG. 15. The pdf of the (top) PDI and (bottom) lowest minimum surface pressure during simulated TCs. Dashed lines = PREIND; solid line indicates 2CO2; dotted line indicates 4CO2.

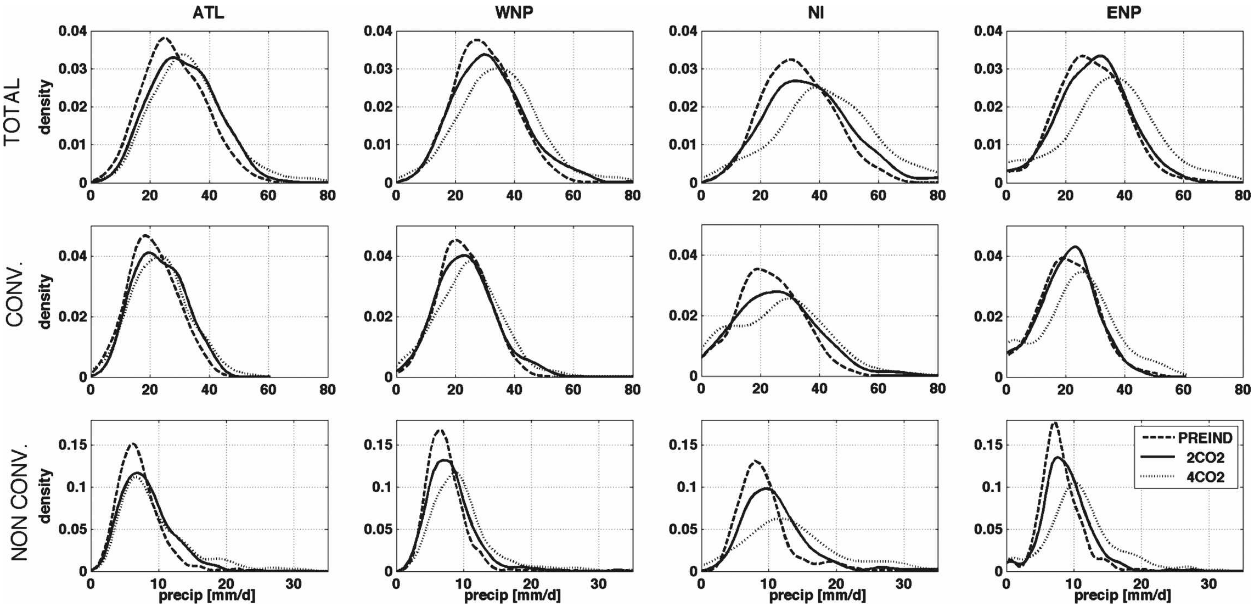

FIG. 16. The pdf of (top) total precipitation, (middle) convective precipitation, and (bottom) large-scale precipitation associated with the simulated TCs in the different regions for the PREIND (dashed line), 2CO2 (solid line), and 4CO2 experiment (dotted line). The x axis is the value of precipitation (mm day^{-1}). The y axis is the (density of) frequency of events corresponding to a certain amount of rainfall.

represents the mean rainfall rate averaged over the TC's lifetime and over the number of TCs for the considered regions. The means have been computed for a domain centered on the core of the cyclones and extending 5° each side. The shaded patterns show the composites of TC rainfall for the PREIND case, whereas the contours are the difference between the composite 2CO2–PREIND (upper panels) and 4CO2–PREIND (lower panels) for the WNP region (left panels) and the ATL region (right panels). Using a bootstrap technique, the changes shown in Fig. 17 are found to be statistically significant, and suggest that the amount of TC rainfall, on average, becomes larger as a consequence of greenhouse warming. These results are consistent with the findings of Knutson and Tuleya (2004), Bengtsson et al. (2007), and Chauvin et al. (2006), for Atlantic hurricanes, and Yoshimura et al. (2006), who used a high-resolution atmospheric-only model.

5. Discussion

In section 4 it was shown that, in general, the frequency of the simulated TCs is substantially and significantly reduced when the concentration of atmospheric CO_2 is increased. To understand this result, we discuss here how global warming affects those characteristics of the tropical atmosphere that are of relevance for the development of TCs. In particular, we consider the two major basic dynamical and thermodynamical mechanisms that can oppose the development, and hence the occurrence, of these phenomena: vertical wind shear and moist atmosphere stability.

It is well known that vertical wind shear is one of the dynamical parameters that controls the formation of TCs. Specifically, strong large-scale vertical wind shear represent unfavorable environmental conditions for the development of TCs (Gray 1968; Emanuel 2003). Therefore, a change in the climatological wind shear induced by greenhouse warming over a certain region might affect the TC frequency there.

Figure 18 shows the vertical wind shear for the PREIND and 4CO2 experiments and the difference 4CO2 − PREIND (for the sake of brevity, we omit the 2CO2 experiment, the results of which are fully consistent with the 4CO2 case, although with smaller amplitudes). Here, the wind shear is defined as the absolute value of the vector wind difference at 300 and 850 hPa [i.e., wind shear = $\sqrt{(u_{300} - u_{850})^2 + (v_{300} - v_{850})^2}$]. In the case of both PREIND and 4CO2, the tropics are characterized by a minimum of vertical wind shear, which is particularly weak in the summer hemisphere. The difference 4CO2 − PREIND (bottom panels) indicates a general reduction of the wind shear over most of the tropics. This result is in agreement with previous studies, which have shown the weakening of the tropi-

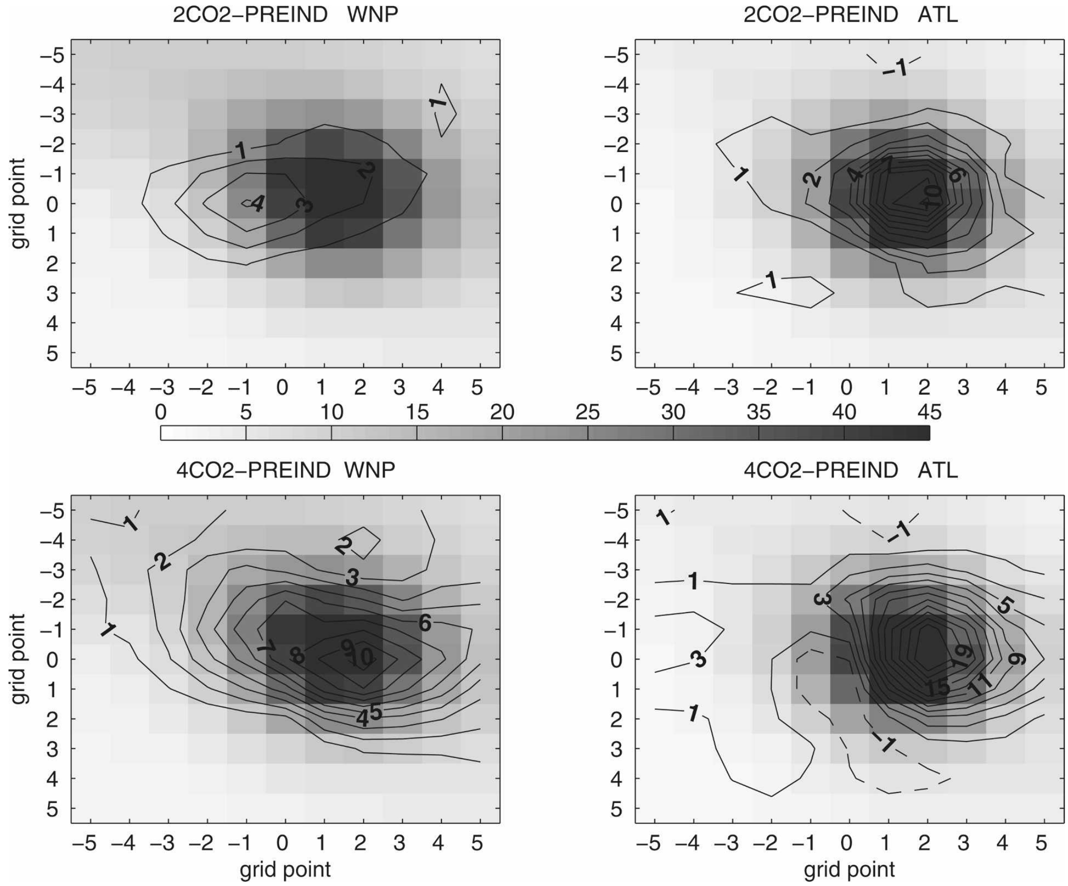

FIG. 17. (left) Composite of TC precipitation for the PREIND experiment over the (left) WNP and (right) ATL region (shaded pattern) along with the difference (top) 2CO2 − PREIND and (bottom) 4CO2 − PREIND shown by the contour patterns. The composites represent the mean rainfall rate averaged over the TC lifetime and over the number of TCs for the considered regions. The means have been computed for a domain centered on the core of the cyclones and extending 5° each side. The PREIND rainfall composite (shaded patterns) have a shaded contour interval of 5 mm day^{-1}. The difference between the 2CO2–PREIND composite and 4CO2–PREIND composite (contour patterns) has a contour interval of 1 mm day^{-1}. The contour lines show only the values that are statistically significant at a 95% level. The significance test has been performed using the bootstrap method.

cal circulation as atmospheric CO_2 increases (e.g., Knutson and Manabe 1995; Vecchi and Soden 2007a).

A notable exception is the reinforcement of the vertical wind shear in the 4CO2 experiment that is visible both in winter and in summer over the north tropical Atlantic. The increase of the tropical Atlantic wind shear in a warmer climate is consistent with the findings of Vecchi and Soden (2007b), and might be one of the possible causes of the TCs reduction found over this area. Interestingly, the warming patterns in the tropical Pacific SSTs found in the 4CO2 case (Fig. 10) resemble the SST anomalies occurring during El Niño events. It is known that ENSO affects TC activity over the north tropical Atlantic, and one hypothesized mechanism is the modulation of the vertical wind shear strength (Goldenberg and Shapiro 1996). Therefore, the stronger response of the tropical eastern Pacific SSTs to global warming might induce a reduction of TC activity in the ATL region possibly through mechanisms similar to the influence exerted by El Niño (see also Aiyyer and Thorncroft 2006; Latif et al. 2007).

The strengthening of the vertical wind shear, however, does not explain the reduction of TCs over the WNP. Figure 18, in fact, shows that the wind shear is reinforced over this region only during the northern winter, whereas it remains substantially unaltered in boreal summer, that is, the active TC season for this area. Therefore, there must be some other explanation for the reduced TC activity here.

Another important parameter that may regulate the development of TCs is the vertical stability of the atmospheric column (e.g., Gray 1979; De Maria et al. 2001). If the atmosphere becomes more stable, the occurrence of phenomena based on the development of

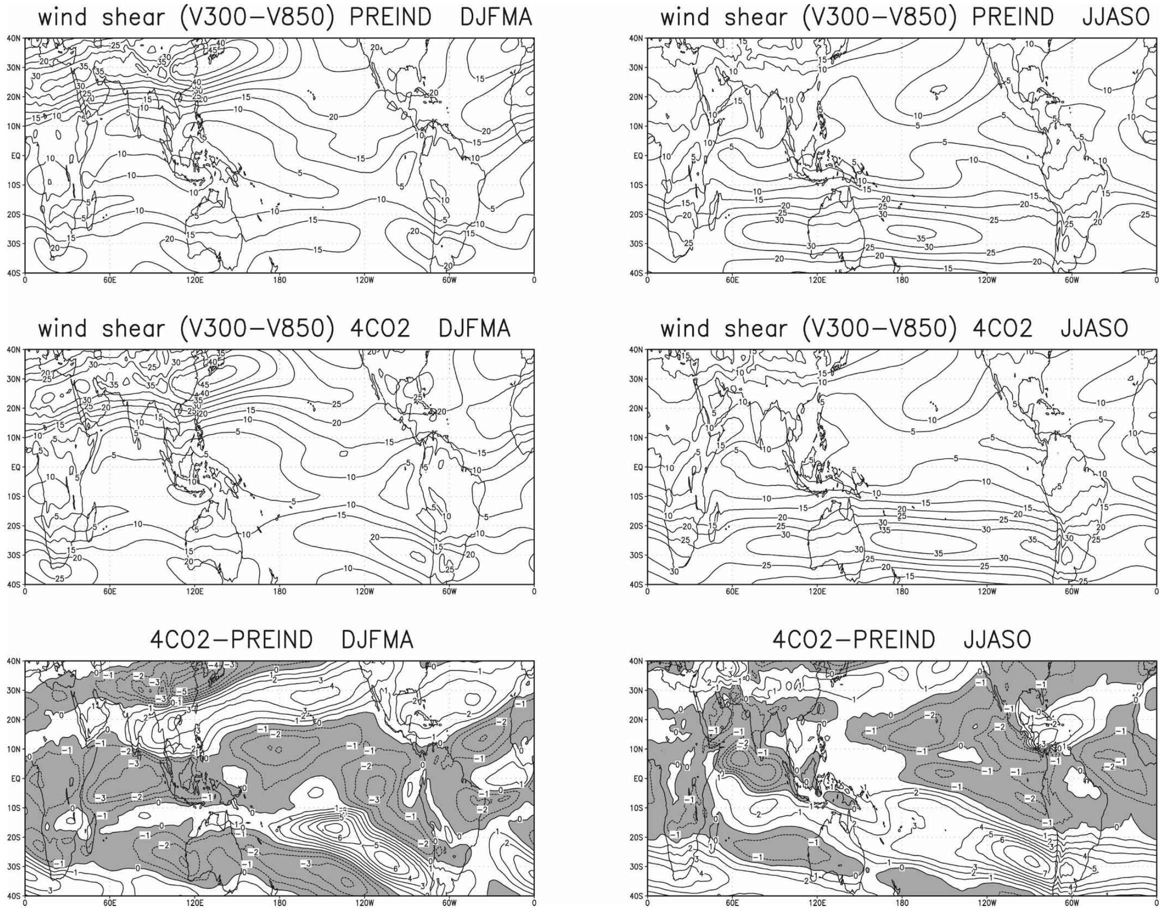

FIG. 18. Seasonal mean of the vertical wind shear defined as the difference between the wind at 300 and at 850 hPa [wind shear = $\sqrt{(u_{300} - u_{850})^2 + (v_{300} - v_{850})^2}$]. The results for the (left) Southern Hemisphere extended summer (DJFMA) and (right) Northern Hemisphere extended summer (JJASO). (top) The fields for the PREIND experiment and (middle) the results from the 4CO2 experiments. For these plots, the contour interval is 5 m s^{-1}. (bottom) The difference between the 4CO2 and the PREIND case. For these plots the contour interval is 1 m s^{-1} and negative values are shaded.

organized convective systems, such as TCs, becomes more unlikely. In section 4a it was shown that the increase of atmospheric CO_2 is accompanied by a reduction of convective precipitation in the tropics. This latter, in turn, might be the sign of an increase in the vertical stability in this region. To investigate possible changes in the stability of the tropical troposphere, we have assessed how the convective available potential energy (CAPE) and the convective inhibition (CIN; Stevens 2005) might be affected by the greenhouse warming.

CAPE and CIN have been defined as

$$\mathrm{CAPE} = \int_{p_{\mathrm{LFC}}}^{p_{\mathrm{LNB}}} R_d (T_{vp} - T_{ve})\, d\ln p$$

$$\mathrm{CIN} = \int_{p_s}^{p_{\mathrm{LFC}}} R_d (T_{vp} - T_{ve})\, d\ln p,$$

where p_s, p_{LFC}, and p_{LNB} are the surface pressure, the pressure of the level of free convection (LFC), and the pressure of the level of neutral buoyancy, respectively; R_d is the dry-air gas constant; and T_{vp} and T_{ve} are the virtual temperature of an air parcel and of the environment (sounding), respectively. CAPE represents the amount of potential energy available for convection, whereas CIN represents the energy used to lift the parcel to the LFC. Thus, CIN can also be interpreted as the potential barrier that has to be overcome in order to initiate convection (see also Emanuel 1994).

The annual mean values of CAPE and CIN have been computed for the three experiments. The results (not shown) indicate that, in general, CAPE tends to increase with increasing CO_2 over most of the tropics. Exceptions are found in the eastern equatorial Indian Ocean, subtropical eastern Pacific and central Atlantic, where a slight reduction of CAPE is recorded. Table 5

TABLE 5. Spatial average of mean CAPE and mean CIN. The mean CAPE and CIN are obtained by averaging over the 30-yr periods of the PREIND, 2CO2, and 4CO2 experiments. The spatial averages are computed over the whole tropical belt (23.5°S–23.5°N) and over the tropical oceans only. Values in parentheses are the percent increment with respect to the PREIND case.

	PREIND	2CO2	4CO2
CAPE tropical mean (J kg^{-1})	109.09	131.39 (+20%)	135.24 (+24%)
CAPE tropical oceans only (J kg^{-1})	132.41	155.21 (+17%)	152.40 (+15%)
CIN tropical mean (J kg^{-1})	13.06	16.04 (+23%)	18.73 (+43%)
CIN tropical oceans only (J kg^{-1})	8.16	9.85 (+21%)	11.46 (+40%)

shows the mean value of CAPE computed over the tropics (23.5°S–23.5°N) and over the tropical oceans only. When the atmospheric CO_2 concentration is doubled, on average CAPE is increased by about 20% over the tropics and 17% over the tropical oceans, with respect to the PREIND case. The further doubling of CO_2 (4CO2) leads to only a slight increase in CAPE (3% with respect to 2CO2 and 24% with respect to PREIND) in the tropical belt. However, something even more interesting is that, over the tropical oceans, the 4CO2 CAPE increases only by about 15% compared to the PREIND value and decreases by about 2% compared to the 2CO2 case. Therefore, the increment of tropical CAPE that appears to accompany the doubling of CO_2 seems to saturate, especially over the oceans, when the CO_2 concentration is further augmented.

Because CAPE increases with the atmospheric CO_2, the lower number of TCs in the 2CO2 and 4CO2 experiments cannot be explained in terms of reduced conditional instability. This result is consistent with Nolan et al. (2007), who found no relationship between CAPE and rate of TC development.

Table 5 also shows the mean value of CIN. Similarly to CAPE, CIN too tends to increase with CO_2 concentration, and at an even greater rate. However, unlike CAPE, CIN does not appear to saturate when the CO_2 concentration is quadrupled. Thus, in the model the increased atmospheric CO_2 leads to an augmented conditional instability (CAPE), but also to an even more pronounced increment of CIN, that is, a higher energy barrier preventing the convection from occurring spontaneously.

Figure 19 shows the pdf of the LFC for the PREIND, 2CO2, and 4CO2 cases over the WNP and ATL areas. The results suggest that the LFC tends to be higher when the atmospheric CO_2 concentration increases. Consistent with the larger CIN, the effect of the higher LFCs is to reduce the chance for convective instabilities to develop.

The generally larger potential energy barrier (CIN) and the shift of the LFC to higher levels, making the development of convective systems less likely, might be responsible for both the general decrease of convective precipitation and, at least in part, for the reduced occurrence of TCs, especially in the WNP region. For the ATL region, on the other hand, the smaller number of TCs appears to be probably due to both the increased vertical wind shear and the reduced instability of the atmosphere.

Importantly, the reduction of the convective activity suggested by this work is fully consistent with the find-

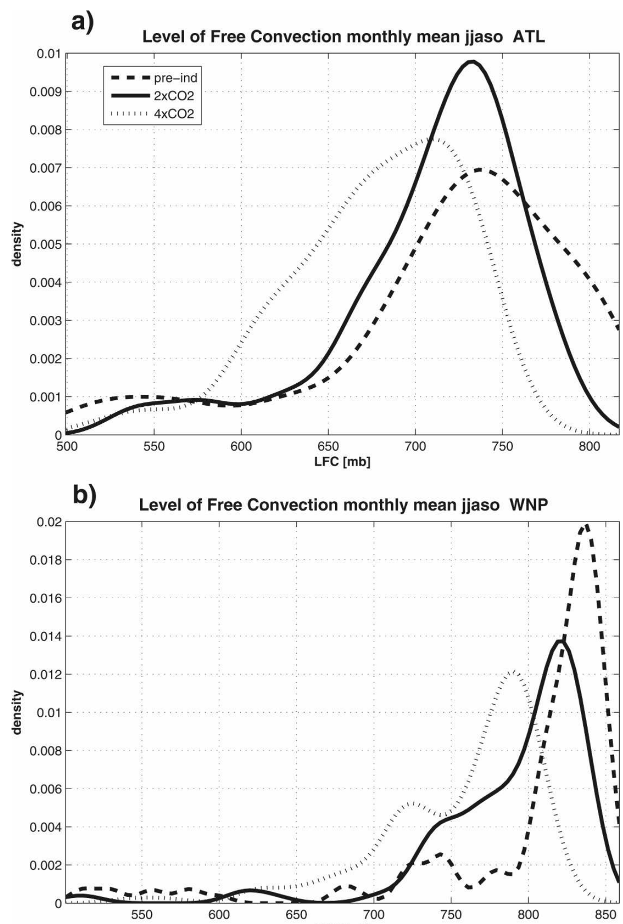

FIG. 19. The pdf of the LFC for the PREIND (dashed), 2CO2 (solid line), and 4CO2 (dotted curve) cases over the (a) ATL region and (b) WNP region during northern summer (JJASO). The *x* axis is the value of vertical levels (hPa), and the *y* axis is the (density of) frequency of occurrence at which free convection can be triggered at that level.

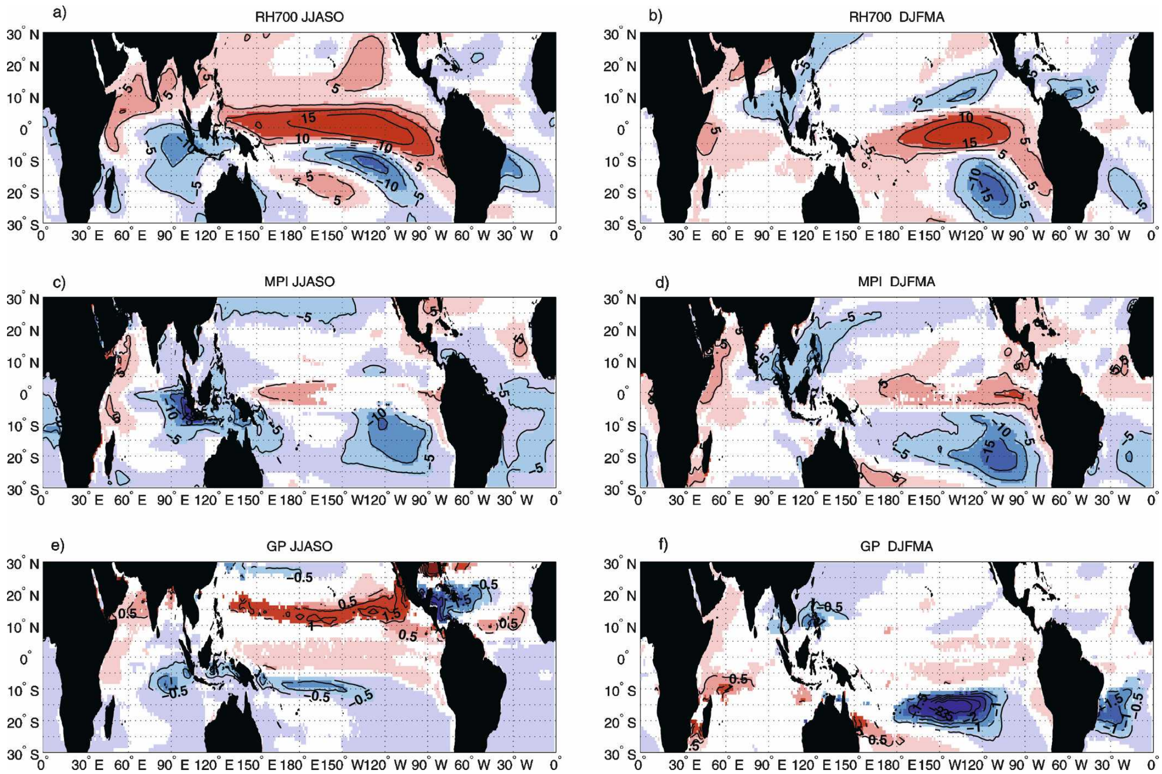

FIG. 20. (a), (b) 4CO2 − PREIND differences of the mean values of RH700, (c), (d) MPI, and (e), (f) GP index. (left) Northern summer and (right) northern winter. The RH is expressed in (number of TC)/(unit area × decade). Only statistically significant at a 95% level contours are shown. The significance test has been performed using the bootstrap method.

ings of other studies investigating the effects of atmospheric CO_2 concentration on tropical convection (e.g., Knutson and Manabe 1995; Sugi and Yoshimura 2004; Held and Soden 2006; Vecchi and Soden 2007a).

The warming of the tropical troposphere is accompanied by an increase of water vapor, especially in the lower layers (not shown), which, in general, leads to an increase of the potential energy available for convection. In fact, as we have seen in Table 5, tropical CAPE increases in the 2CO2 and 4CO2 experiments, compared with the PREIND case. Therefore, when convection occurs it has more potential energy available and the events may be more intense. In other words, the increase in CIN makes the triggering of convective episodes more difficult, but the larger CAPE makes the convective episodes stronger. This might explain the increased intensity of TC precipitation, found in section 4b (Figs. 16 and 17).

To substantiate our findings further, we have assessed how other (empirical) indices related to the TC activity are changed as a consequence of greenhouse warming. Specifically, parameters like the midtropospheric relative humidity over the oceans, the maximum potential index (MPI; Bister and Emanuel 2002), and the genesis potential (GP) index (Emanuel and Nolan 2004) have been found to be related with TC activity (e.g., Camargo et al. 2004). In Fig. 20 we show the differences between the 30-yr mean values of these parameters from the 4CO2 and the PREIND case.

The tropical mean of the 4CO2 − PREIND difference of the 700-hPa relative humidity (RH700) exhibits a very small increase, consistent with Held and Soden (2006). However, locally some considerable change is visible (Fig. 20, upper panels). A substantial increase, for example, is found in the equatorial band of the Pacific Ocean, whereas reductions are found in the tropical Indian Ocean and subtropical Pacific and Atlantic Oceans. In northern summer (left panel), the RH700 appears to decrease in the North Atlantic, whereas a very slight increase is found in the WNP region.

When averaged over the tropics, the MPI difference (Figs. 20c,d) shows a reduction of this index. Consistent with Vecchi and Soden (2007b), the patterns of MPI change are similar to the patterns of SST change (Fig. 10). MPI increases (decreases) over the region where the SST warming is more (less) intense. Thus, a substantial increase of MPI is found in the equatorial Pacific and western Indian Ocean, while the index decreases over the southern Pacific, eastern Indian

Ocean, WNP, and tropical Atlantic, especially during northern summer (left panel).

The 4CO2 − PREIND difference of the GP index (lower panels) reveals an increase of this parameter in the tropical Pacific, north of the equator, during the northern summer. In most of the WNP sector, the difference is not statistically significant, though there is a portion of the region where the GP exhibits a significant increment. The increase is more pronounced in the central-eastern North Pacific. Notably, from the results shown in section 4 (e.g., Fig. 12), this is also the region where TC activity does not appear to be reduced by the CO_2 increase.

Overall, the results obtained from the parameters shown in Fig. 20 are consistent with the findings that we obtained with the TC tracking methods described in section 2d. The agreement appears to be particularly evident in the ATL region, where all of the empirical parameters suggest a reduction of TC activity, consistent with the results shown in section 4. In the WNP area, on the other hand, the agreement is less obvious. While the MPI shows a slight but visible decrease, the GP index exhibits some increase, especially in the eastern part.

6. Summary

In this study, a fully coupled high-resolution AOGCM has been used to investigate the possible impact of greenhouse global warming on the characteristics of tropical cyclones.

The simulated TCs have many basic, gross features similar to the observed ones. However, the rather low intensity of the low-level winds and the too large distance between the cyclone eye and the wind maximum remain unsatisfactory. These shortcomings are most likely due to the model resolution, which, although rather high for long climate simulations, is still too coarse for an adequate representation of the tight structures accompanying these phenomena. Despite these problems, the model seems to be able to simulate a reasonable realistic climatology of TCs in terms of spatial distribution, and seasonal and interannual variability of TC activity. In particular, the model appears to capture at least some of the links between SST interannual variability and TC activity.

The enhanced concentration of atmospheric CO_2 induces a warming of the entire tropical and subtropical upper ocean, accompanied by a redistribution of tropical rainfall. The increase of the tropical ocean surface temperature, however, is not uniform, and the eastern Pacific exhibits a more pronounced warming with patterns that resemble El Niño SST anomalies. The total precipitation averaged over the tropics increases with the CO_2 increase, but the convective precipitation exhibits a significant reduction.

Along with the attenuated convective activity, our simulations show a substantial and significant reduction of the number of generated TCs, especially over the northwest Pacific and North Atlantic tropical regions. Both the decrease in convective activity and the reduced occurrence of TCs might be due to the larger potential energy barrier found when the CO_2 concentration is increased. In the reduction of the TC activity in the ATL region, however, an important role also appears to be played by a considerable increase in vertical wind shear.

Greenhouse warming is associated with a poleward expansion of the tropical warm SSTs. In particular, the 26°C isotherm, which appears to be crucial for the development of TCs in the present climate, in the 4CO2 case migrates poleward by almost 10° latitude when compared to the PREIND one. In the model, however, the warming of the subtropical and midlatitudes is not accompanied by a poleward extension of TC action, consistent with earlier works. The peaks of TC activity remain substantially confined equatorward of 20° latitude in both hemispheres.

Despite the reduced number of TCs generated when the CO_2 has doubled and quadrupled, there is evidence of an increase in their intensity in terms of precipitation. This might be related with the increase of CAPE found in the warmer climate. The intensity of the simulated TCs expressed in terms of near-surface wind (PDI) and surface pressure, on the other hand, does not appear to be significantly affected by the global warming. However, this result is probably related to the deficiencies that the model exhibits in reproducing realistic TC intensities.

Acknowledgments. The authors are indebted to Andrea Alessandri, Chiara Cagnazzo, and Gabriel Vecchi for their precious help, useful suggestions, and stimulating discussions. They also want to thank the three anonymous reviewers for their suggestions and constructive criticisms and K. Emanuel for making available the routines to compute the maximum potential index (online at http://wind.mit.edu/emanuel/home.html). This work has been supported by the Euro-Mediterranean Centre for Climate Change and by the European Community project ENSEMBLES, Contract GOCE-CT-2003-505539.

REFERENCES

Aiyyer, A. R., and C. Thorncroft, 2006: Climatology of vertical wind shear over the tropical Atlantic. *J. Climate,* **19,** 2969–2983.

Anthes, R. A., R. W. Corell, G. Holland, J. W. Hurrel, M. C. MacCracken, and K. E. Trenberth, 2006: Hurricanes and global warming—Potential linkages and consequences. *Bull. Amer. Meteor. Soc.,* **87,** 623–628.

Behera, S. K., J. J. Luo, S. Masson, P. Delecluse, S. Gualdi, A. Navarra, and T. Yamagata, 2005: Paramount impact of the Indian Ocean dipole on the East African short rains: A CGCM study. *J. Climate,* **18,** 4514–4530.

Bengtsson, L., M. Botzet, and M. Esch, 1995: Hurricane–type vortices in a general–circulation model. *Tellus,* **47A,** 175–196.

——, ——, and ——, 1996: Will greenhouse gas–induced warming over the next 50 years lead to higher frequency and greater intensity of hurricanes? *Tellus,* **48A,** 57–73.

——, K. I. Hodges, M. Esch, N. Keenlyside, L. Kornblueh, J.-J. Luo, and T. Yamagata, 2007: How may tropical cyclones change in a warmer climate? *Tellus,* **59A,** 539–561.

Bister, M., and K. A. Emanuel, 2002: Low frequency variability of tropical cyclone potential intensity 1. Interannual to interdecadal variability. *J. Geophys. Res.,* **107,** 4801, doi:10.1029/2001JD000776.

Blanke, B., and P. Delecluse, 1993: Low frequency variability of the tropical Atlantic Ocean simulated by a general circulation model with mixed layer physics. *J. Phys. Oceanogr.,* **23,** 1363–1388.

Broccoli, A. J., and S. Manabe, 1990: Can existing climate models be used to study anthropogenic changes in tropical cyclone climate. *Geophys. Res. Lett.,* **17,** 1917–1920.

Camargo, S. J., A. G. Barnston, and S. E. Zebiak, 2004: Properties of tropical cyclones in atmospheric general circulation models. International Research Institute for Climate Prediction Tech. Rep. 04-02, 72 pp.

Chan, J. C.-L., 2000: Tropical cyclone activity over the western North Pacific associated with El Niño and La Niña events. *J. Climate,* **13,** 2960–2972.

Chauvin, F., J.-F. Royer, and M. Deque, 2006: Response of hurricane-type vortices to global warming as simulated by ARPEGE-Climat at high resolution. *Climate Dyn.,* **27,** 377–399.

Chia, H. H., and C. F. Ropelewski, 2002: The interannual variability in the genesis location of tropical cyclones in the northwest Pacific. *J. Climate,* **15,** 2934–2944.

Delworth, T. L., and M. E. Mann, 2000: Observed and simulated multidecadal variability in the Northern Hemisphere. *Climate Dyn.,* **16,** 661–676.

De Maria, M., J. A. Knaff, and B. H. Connell, 2001: A tropical cyclone genesis parameter for the tropical Atlantic. *Wea. Forecasting,* **16,** 219–233.

Dutton, J. F., C. J. Poulsen, and J. L. Evans, 2000: The effect of global climate change on the region of tropical convection in CSM1. *Geophys. Res. Lett.,* **27,** 3049–3052.

Elsner, J. B., and B. Kocher, 2000: Global tropical cyclone activity: A link to the North Atlantic Oscillation. *Geophys. Res. Lett.,* **27,** 129–132.

Emanuel, K. A., 1987: The dependence of hurricane intensity on climate. *Nature,* **326,** 483–485.

——, 1994: *Atmospheric Convection.* Oxford University Press, 580 pp.

——, 2003: Tropical cyclones. *Annu. Rev. Earth Planet. Sci.,* **31,** 75–104.

——, 2005: Increasing destructiveness of tropical cyclones over the past 30 years. *Nature,* **436,** 686–688.

——, and D. S. Nolan, 2004: Tropical cyclone activity and global climate. Preprints, *26th Conf. on Hurricanes and Tropical Meteorology,* Miami, FL, Amer. Meteor. Soc., 10A.2. [Available online at http://ams.confex.com/ams/pdfpapers/75463.pdf.]

Fichefet, T., and M. A. Morales-Maqueda, 1999: Modelling the influence of snow accumulation and snow–ice formation on the seasonal cycle of the Antarctic sea-ice cover. *Climate Dyn.,* **15,** 251–268.

Frank, W. M., 1977: The structure and energetics of the tropical cyclone I. The storm structure. *Mon. Wea. Rev.,* **105,** 1119–1135.

——, and G. S. Young, 2007: The interannual variability of tropical cyclones. *Mon. Wea. Rev.,* **135,** 3587–3598.

Gent, P. R., and J. C. McWilliams, 1990: Isopycnal mixing in ocean circulation models. *J. Phys. Oceanogr.,* **20,** 150–155.

Goldenberg, S. B., and L. J. Shapiro, 1996: Physical mechanisms for the association of El Niño and West African rainfall with Atlantic major hurricane activity. *J. Climate,* **9,** 1169–1187.

——, C. W. Landsea, A. M. Mestas-Nuñez, and W. M. Gray, 2001: The recent increase in the Atlantic hurricane activity: Causes and implications. *Science,* **293,** 474–479.

Gray, W. M., 1968: Global view of the origin of tropical disturbances and storms. *Mon. Wea. Rev.,* **96,** 669–700.

——, 1979: Hurricanes: Their formation, structure and likely role in the tropical circulation. *Meteorology over the Tropical Oceans,* D. B. Shaw, Ed., Royal Meteorological Society, 155–218.

——, 1984: Atlantic seasonal hurricane frequency. Part I: El Niño and 30-mb quasi-biennial oscillation influences. *Mon. Wea. Rev.,* **112,** 1649–1668.

Gualdi, S., A. Navarra, E. Guilyardi, and P. Delecluse, 2003a: Assessment of the tropical Indo-Pacific climate in the SINTEX CGCM. *Ann. Geophys.,* **46,** 1–26.

——, E. Guilyardi, A. Navarra, S. Masina, and P. Delecluse, 2003b: The interannual variability in the tropical Indian Ocean as simulated by a CGCM. *Climate Dyn.,* **20,** 567–582.

Guilyardi, E., P. Delecluse, S. Gualdi, and A. Navarra, 2003: Mechanisms for ENSO phase change in a coupled GCM. *J. Climate,* **16,** 1141–1158.

Haarsma, R. J., J. F. B. Mitchell, and C. A. Senior, 1993: Tropical disturbances in a GCM. *Climate Dyn.,* **8,** 247–257.

Held, I. M., and B. J. Soden, 2006: Robust responses of the hydrological cycle to global warming. *J. Climate,* **19,** 5686–5699.

——, M. Zhao, and B. Wyman, 2007: Dynamic radiative–convective equilibria using GCM column physics. *J. Atmos. Sci.,* **64,** 228–238.

Henderson-Sellers, A., and Coauthors, 1998: Tropical cyclones and global climate change: A post-IPCC assessment. *Bull. Amer. Meteor. Soc.,* **79,** 19–38.

Holland, G. J., 1993: Ready reckoner. Global Guide to Tropical Cyclone Forecasting, World Meteorological Organization, WMO/TC 560, Report TCP-31. [Available online at http://www.bom.gov/au/bmrc/pubs/tcgnide/globa_guide_intro.htm.]

——, 1997: The maximum potential intensity of tropical cyclones. *J. Atmos. Sci.,* **54,** 2519–2541.

Jones, P. D., D. E. Parker, T. J. Osborn, and K. R. Briffa, 2006: Global and hemispheric temperature anomalies—Land and marine instrumental records. Trends: A Compendium of Data on Global Change, Carbon Dioxide Information Analysis Center, Oak Ridge National Laboratory, U.S. Department of Energy. [Available online at http://cdiac.ornl.gov/trends/temp/jonescru/jones.html.]

Knutson, T. R., and S. Manabe, 1995: Time–mean response over the tropical Pacific to increased CO_2 in a coupled ocean–atmosphere model. *J. Climate,* **8,** 2181–2199.
——, and R. E. Tuleya, 2004: Impact of CO_2 induced warming on simulated hurricane intensity and precipitation: Sensitivity to the choice of climate model and convective parameterization. *J. Climate,* **17,** 3477–3495.
——, and ——, 2005: Reply. *J. Climate,* **18,** 5183–5187.
——, ——, W. Shen, and I. Ginis, 2001: Impact of CO_2–induced warming on hurricane intensities simulated in a hurricane model with ocean coupling. *J. Climate,* **14,** 2458–2468.
Landsea, C. W., 2007: Counting Atlantic tropical cyclones back to 1900. *Eos, Trans. Amer. Geophys. Union,* **88,** 197–202.
——, B. A. Harper, K. Hoarau, and J. Knaff, 2006: Can we detect trends in extreme tropical cyclones? *Science,* **313,** 452–454.
Latif, M., N. Keenlyside, and J. Bader, 2007: Tropical sea surface temperature, vertical wind shear, and hurricane development. *Geophys. Res. Lett.,* **34,** L01710, doi:10.1029/2006GL027969.
Luo, J.-J., S. Masson, S. Behera, P. Delecluse, S. Gualdi, A. Navarra, and T. Yamagata, 2003: South Pacific origin of the decadal ENSO-like variation as simulated by a coupled GCM. *Geophys. Res. Lett.,* **30,** 2250, doi:10.1029/2003GL018649.
Madec, G., P. Delecluse, M. Imbard, and C. Levy, 1998: OPA 8.1 Ocean General Circulation Model reference manual. Institut Pierre-Simon Laplace Internal Rep. 11, 91 pp.
Masson, S., and Coauthors, 2005: Impact of barrier layer on winter-spring variability of the southeastern Arabian Sea. *Geophys. Res. Lett.,* **32,** L07703, doi:10.1029/2004GL021980.
McDonald, R. E., D. G. Bleaken, D. R. Cresswell, V. D. Pope, and C. A. Senior, 2005: Tropical storms: Representation and diagnosis in climate models and impacts of climate change. *Climate Dyn.,* **25,** 19–36.
Michaels, P. J., P. C. Knappenberger, and C. Landsea, 2005: Comments on "Impacts of CO_2–induced warming on simulated hurricane intensity and precipitation: Sensitivity to the choice of climate model and convective scheme." *J. Climate,* **18,** 5179–5182.
Morcrette, J. J., 1991: Radiation and cloud radiative properties in the European Centre for Medium Range Weather Forecasts forecasting system. *J. Geophys. Res.,* **96,** 9121–9132.
Nolan, D. S., E. D. Rappin, and K. A. Emanuel, 2007: Tropical cyclogenesis sensitivity to environmental parameters in radiative-convective equilibrium. *Quart. J. Roy. Meteor. Soc.,* **133,** 2085–2107.
Nordeng, T. E., 1994: Extended versions of the convective parameterization scheme at ECMWF and their impact on the mean and transient activity of the model in the Tropics. ECMWF Research Department Tech. Memo. 206, 41 pp.
Oouchi, K., J. Yoshimura, H. Yoshimura, R. Mizuta, S. Kusunoki, and N. A. Noda, 2006: Tropical cyclone climatology in a global-warming climate as simulated in a 20 km-mesh global atmospheric model: Frequency and wind intensity analyses. *J. Meteor. Soc. Japan,* **84,** 259–276.
Palmen, E., 1948: On the formation and structure of tropical hurricanes. *Geophysica,* **3,** 26–39.
Pezza, A. B., and I. Simmonds, 2005: The first South Atlantic hurricane: Unprecedented blocking, low shear and climate change. *Geophys. Res. Lett.,* **32,** L15712, doi:10.1029/2005GL023390.
Pielke, R., Jr., C. Landsea, M. Mayfield, J. Laver, and R. Pasch, 2005: Hurricanes and global warming. *Bull. Amer. Meteor. Soc.,* **86,** 1571–1575.
——, ——, ——, ——, and ——, 2006: Reply. *Bull. Amer. Meteor. Soc.,* **87,** 628–631.
Rayner, N. A., D. E. Parker, E. B. Horton, C. K. Folland, L. V. Alexander, D. P. Rowell, E. C. Kent, and A. Kaplan, 2003: Global analyses of sea surface temperature, sea ice, and night marine air temperature since the late nineteenth century. *J. Geophys. Res.,* **108,** 4407, doi:10.1029/2002JD002670.
Roeckner, E., and Coauthors, 1996: The atmospheric general circulation model Echam-4: Model description and simulation of present-day climate. Max-Planck-Institut für Meteorologie Rep. 218, 90 pp.
Roullet, G., and G. Madec, 2000: Salt conservation, free surface, and varying levels: A new formulation for ocean general circulation models. *J. Geophys. Res.,* **105,** 23 927–23 942.
Royer, J.-F., F. Chauvin, B. Timbal, P. Araspin, and D. Grimal, 1998: A GCM study of the impact of greenhouse gas increase on the frequency of occurrence of tropical cyclones. *Climate Dyn.,* **38,** 307–343.
Stevens, B., 2005: Atmospheric moist convection. *Annu. Rev. Earth Planet. Sci.,* **33,** 605–643.
Sugi, M., and J. Yoshimura, 2004: A mechanism of tropical precipitation change due to CO_2 increase. *J. Climate,* **17,** 238–243.
——, A. Noda, and N. Sato, 2002: Influence of global warming on tropical cyclone climatology: An experiment with the JMA global model. *J. Meteor. Soc. Japan,* **80,** 249–272.
Tiedtke, M., 1989: A comprehensive mass flux scheme for cumulus parameterization in large–scale models. *Mon. Wea. Rev.,* **117,** 1779–1800.
Timmermann, R., H. Goosse, G. Madec, T. Fichefet, C. Ethe, and V. Dulie're, 2005: On the representation of high latitude processes in the ORCALIM global coupled sea ice-ocean model. *Ocean Modell.,* **8,** 175–201.
Trenberth, K., 2005: Uncertainty in hurricanes and global warming. *Science,* **308,** 1753–1754.
Valcke, S., L. Terray, and A. Piacentini, 2000: The OASIS coupler user guide version 2.4. CERFACS Tech. Rep. TR/CMGC/00-10, 85 pp.
Vecchi, G. A., and B. J. Soden, 2007a: Global warming and the weakening of the tropical circulation. *J. Climate,* **20,** 4316–4340.
——, and ——, 2007b: Increased tropical Atlantic wind shear in model projections of global warming. *Geophys. Res. Lett.,* **34,** L08702, doi:10.1029/2006GL028905.
Walsh, K. J. E., 1997: Objective detection of tropical cyclones in high-resolution analyses. *Mon. Wea. Rev.,* **125,** 1767–1779.
——, 2004: Tropical cyclones and climate change: Unresolved issues. *Climate Res.,* **22,** 77–83.
——, and B. F. Ryan, 2000: Tropical cyclone intensity increase near Australia as a result of climate change. *J. Climate,* **13,** 3029–3036.
Webster, P. J., G. J. Holland, J. A. Curry, and H.-R. Chang, 2005: Changes in tropical cyclones number, duration and intensity in a warming environment. *Science,* **309,** 1844–1846.
Willoughby, H. E., J. A. Clos, and M. G. Shoreibah, 1982: Concentric eye walls, secondary wind maxima, and the evolution of the hurricane vortex. *J. Atmos. Sci.,* **39,** 395–411.
Xie, P., and P. Arkin, 1997: Global precipitation: A 17-year monthly analysis based on gauge observations, satellite estimates, and numerical model outputs. *Bull. Amer. Meteor. Soc.,* **78,** 2539–2558.
Yoshimura, J., M. Sigu, and A. Noda, 2006: Influence of greenhouse warming on tropical cyclone frequency. *J. Meteor. Soc. Japan,* **84,** 405–428.